J. Astrophys. Astr. (2004) **25,** 143–183

A High Galactic Latitude HI 21 cm-line Absorption Survey using the GMRT: I. Observations and Spectra

Rekhesh Mohan*[1], K. S. Dwarakanath[2] & G. Srinivasan[3]
Raman Research Institute, Bangalore 560 080, India.
[1]*e-mail: reks@iiap.res.in*
[2]*e-mail: dwaraka@rri.res.in*
[3]*e-mail: srini@rri.res.in*

Received 2004 June 4; accepted 2004 November 3

Abstract. We have used the Giant Meterwave Radio Telescope (GMRT) to measure the Galactic HI 21-cm line absorption towards 102 extragalactic radio continuum sources, located at high ($|b| > 15^\circ$) Galactic latitudes. The Declination coverage of the present survey is $\delta \gtrsim -45^\circ$. With a mean rms optical depth of ~ 0.003, this is the most sensitive Galactic HI 21-cm line absorption survey to date. To supplement the absorption data, we have extracted the HI 21-cm line emission profiles towards these 102 lines of sight from the Leiden Dwingeloo Survey of Galactic neutral hydrogen. We have carried out a Gaussian fitting analysis to identify the discrete absorption and emission components in these profiles. In this paper, we present the spectra and the components. A subsequent paper will discuss the interpretation of these results.

Key words. ISM: clouds, kinematics and dynamics—radio lines: ISM.

1. Introduction

The distribution atomic hydrogen in the Galaxy and its physical properties have been extensively studied. Soon after the discovery of the HI 21-cm line, a number of single dish HI surveys were conducted (see Burton 1988 for a useful compilation of the early HI surveys). The single dish HI absorption spectra are limited by the errors due to the variation of HI emission intensity over the angular scales smaller than the telescope beam. Interferometric surveys are a better alternative for HI absorption studies. An interferometer rejects the low spatial frequencies where HI emission is dominant, resulting in reliable absorption spectra. There have been a number of interferometric HI absorption studies, often supplemented by single dish observations to measure the HI emission.

The early HI 21-cm line absorption and emission studies led to the emergence of a global picture of the interstellar medium (Clark, Radhakrishnan & Wilson 1962; Clark 1965). These and later studies paved the way for the models of the interstellar medium of the Galaxy. Field, Goldsmith & Habbing (1969) modeled the ISM as cool

*Currently at the Indian Institute of Astrophysics, Bangalore 560 034, India.

dense concentrations of gas, often referred to as "interstellar clouds" (the Cold Neutral Medium or CNM) in pressure equilibrium with a warmer intercloud medium (the Warm Neutral Medium or WNM). While this initial model of the ISM has been refined considerably by later studies (Wolfire *et al* 1995), the basic picture of the ISM with cold diffuse clouds and a warmer intercloud medium has survived. The spin temperature of the cold clouds which constitute the CNM was estimated to be ~ 80 K and that of the WNM to be ~ 8000 K. The cold clouds manifest as narrow Gaussian features with typical velocity dispersions of a few km s^{-1} in both HI emission and absorption profiles. The intercloud medium, on the other hand, is identified with broad Gaussian features with typical velocity dispersions $\gtrsim 10$ km s^{-1}. The intercloud medium is usually detected in emission, since the HI absorption in the warm gas is very weak. We summarize the results from some of the important surveys below.

Radhakrishnan *et al*. (1972a, b) used the Parkes Interferometer to study the HI absorption towards 35 extragalactic radio sources, in the Galactic latitude range $6^\circ \leq |b| \leq 74^\circ$ and 53 Galactic radio sources in the lower Galactic latitudes, mostly located at $|b| < 2^\circ$. In addition, the Parkes 64 m telescope was used to obtain the HI emission towards all these directions. The velocity resolution of these observations was 2.1 km s^{-1}. The rms noise in the HI optical depth profiles varied from ~ 0.01 to > 0.1, depending on the flux density of the background source. They concluded that the HI absorption features arise in discrete concentrations of gas with a spin temperature in the range 60–80 K. They also derived the number density of these features to be ~ 2.5 per Kpc (Radhakrishnan & Goss 1972). The number of such concentrations of gas for a given optical depth τ was $\propto e^{-\tau}$. Lack of absorption in the intercloud medium, which was identified as the wide "shoulders" in HI emission profiles, enabled them to put a limit of > 750 K for the spin temperature of this gas.

Dickey & Benson (1982) used the NRAO 300 ft and 140 ft telescopes as an interferometer to detect absorption in the 21-cm line towards 64 radio continuum sources. The HI emission profiles were obtained using the 300 ft telescope alone. These sources were both Galactic and extragalactic and spread over a range of latitudes $0^\circ \lesssim |b| \lesssim 70^\circ$. They have produced HI absorption profiles with an rms optical depth in the range ~ 0.007–0.16, with a velocity resolution ranging from $1.3 - 5.3$ km s^{-1}. Among the main results of this study was the realization that for lower Galactic latitudes ($|b| \lesssim 15^\circ$), HI emission surveys using single dish telescopes would miss a significant amount of gas ($\sim 40\%$) due to HI self absorption, wherein the cold HI gas in the foreground absorbs the HI line emission from the background gas. They also found more HI gas with lower spin temperature ($100 \lesssim T_S \lesssim 150$ K) at lower latitudes ($|b| < 2^\circ$) as compared to the previous HI line surveys. They concluded that such a behaviour is the result of velocity blending.

Mebold *et al*. (1981) carried out an HI absorption survey towards 69 sources in the range $0^\circ \lesssim |b| \lesssim 80^\circ$ using the NRAO 3-element interferometer. They obtained the corresponding HI emission using the Effelsberg 100 m telescope, the 91 m Green Bank telescope or the 64 m Parkes telescope. The velocity resolution of these profiles were in the range 0.42–3.3 km s^{-1}. These profiles, on an average, had an rms in HI optical depth $\gtrsim 0.05$. They found most of the HI absorption features to have a spin temperature in the range 20 to 140 K. For the HI absorption data at $|b| > 15^\circ$, they found indications for a bimodal distribution in the radial velocity distribution of absorbing features. However, since the number of components at higher radial velocities were small, they were unable to study its significance.

Till recently, the Very Large Array (VLA) used to be the only instrument with a collecting area comparable with large single dish telescopes. The survey by Dickey *et al.* (1983) using the VLA is limited to lower Galactic latitudes ($|b| < 10^\circ$). Moreover, the optical depth detection limit for this survey is ~ 0.1 (3σ). From the various HI absorption surveys carried out so far (Radhakrishnan *et al.* 1972a, b; Mebold *et al.* 1981; Dickey & Benson 1982 ; Dickey *et al.* 1983), more than 600 absorption spectra are available, but the optical depth detection limits of more than 75% of these are above 0.1. From the available results, the cloud population observed in HI absorption seem to have a Gaussian random velocity distribution. The dispersion in the random velocities of HI absorption features is $\sim 7\,\mathrm{km\ s^{-1}}$ (Dickey & Lockman 1990, and references therein).

The low optical depth regime of Galactic HI is largely unexplored except for the HI absorption studies using the Arecibo reflector by Dickey *et al.* (1978) and more recently by Heiles & Troland (2003a, b). Dickey *et al.* measured HI absorption and emission towards 27 extragalactic radio continuum sources located at high and intermediate Galactic latitudes ($|b| > 5^\circ$). The rms optical depth in their spectra were typically ~ 0.005. In many of the profiles the systematics in the band dominate the noise in the spectrum. As we noted earlier, these observations are not impervious to HI emission fluctuations introducing errors in the absorption profile (Dickey & Lockman 1990). Radhakrishnan & Goss (1972) found the number of HI absorption features for a given optical depth, τ to be proportional to $e^{-\tau}$. However, the data by Dickey *et al.* (1978) as well as the later survey using the Green Bank Interferometer (Mebold *et al.* 1982) indicated that for $|b| > 15^\circ$ this dependence is steeper than $e^{-\tau}$. This trend was explained as due to increase of low optical depth features with increasing angular and velocity resolution (Mebold *et al.* 1982). Dickey *et al.* (1978) also noted that the velocity distribution of HI absorption features is dependent on the optical depth. For the optically thin clouds ($\tau < 0.1$), the velocity dispersion was $\sim 11\,\mathrm{km\ s^{-1}}$, whereas for the optically thick clouds ($\tau > 0.1$) this value is $\sim 6\,\mathrm{km\ s^{-1}}$. Heiles & Troland (2003a, b) analysed HI absorption and emission profiles toward 79 lines of sight. A good fraction of these directions (66 out of 79) were at Galactic latitudes $|b| > 10^\circ$. They found evidence for an excess of low column density ($N_{\rm HI} < 5 \times 10^{19}\,\mathrm{cm^{-2}}$) CNM components.

2. Motivations for the present survey

The prime motivation for the present survey was to obtain sensitive HI absorption measurements at high Galactic latitudes and to study the random velocity distribution of HI clouds. Although there exist extensive data on Galactic HI absorption, there is a lack of sensitive HI absorption studies. There are indications that the low optical depth features ($\tau < 0.1$) form a distinct class (Dickey *et al.* 1978; Mebold *et al.* 1982; Heiles & Troland 2003b), with larger velocity dispersion. The dependence of HI column density and optical depths of these clouds on their random velocities are not well studied. Our aim was to investigate the nature of low optical depth HI features in the Galaxy and to estimate their velocity distribution. One of the difficulties encountered in studying discrete components in the HI 21 cm-line profiles in the Galactic plane is the plethora of absorption lines. Larger path length through the disk of the Galaxy results in larger number of absorption components. In such cases, the available techniques often result in more than one possible solution for the parameters of individual

features. Moreover, the observed radial velocities are usually the sum of components arising from random motion and the differential rotation of the Galaxy. The distances to the absorbing clouds are seldom known. Hence the systematic component in the observed radial velocity arising from Galaxy's rotation is unknown. Therefore, the lower Galactic latitudes are not suitable for a survey to search for low optical depth components and to study the random velocity distribution of interstellar clouds. We have chosen a lower cutoff of 15° for the Galactic latitude in our observations.

Most of the HI gas at higher latitudes is observed only in HI emission (Dickey & Lockman 1990, and references therein). The HI emission profiles often show components at velocities that cannot arise from Galactic rotation. The existing surveys of HI absorption indicate that there is very little absorption in directions above a latitude of $\sim 45°$, down to optical depths ~ 0.01 (Dickey *et al*. 1978). But, there are indications that HI gas layer of the Galaxy extends to several kpc (Albert 1983; Lockman & Gehman 1991; Kalberla *et al*. 1998). A more sensitive HI absorption search is required to understand the nature of this gas and to characterize it.

We present here the HI absorption measurements with the Giant Metrewave Radio Telescope (GMRT) towards 102 extragalactic radio continuum sources located at intermediate and high latitudes. The present survey, with an rms detection limit of 0.003 in HI optical depth is at least a factor of 5 more sensitive than the existing interferometric surveys and is comparable with the sensitivities achieved in the single dish HI surveys using the Arecibo telescope (Dickey *et al*. 1978; Heiles & Troland 2003a). An overview of the GMRT is given in the next section. The strategy for selecting the sources is outlined in section 4. and the details pertaining to the observations are given in section 5.. A brief description of the data analysis is given in section 6. and section 7. describes a sample HI absorption profile. The list of observed sources is presented in Appendix A, the HI line profiles towards these sources are given in Appendix B, and Appendix C lists the discrete HI features identified from each of these profiles.

3. The Giant Meterwave Radio Telescope

The Giant Meterwave Radio Telescope (GMRT) consists of 30 fully steerable dishes, of 45 meter diameter with a maximum baseline of 25 km (Swarup *et al*. 1991). The aperture efficiency of the dishes is $\sim 40\%$ in the 21 cm band, which implies an effective collecting area of $\sim 19000\,\mathrm{m}^2$. The full width at half maximum of the primary beam is $\sim 25'$ and that of the synthesized beam is $\sim 2''$ (uniform weighting) at 1.4 GHz. The 21 cm receiver is a wide band system covering the frequency range 900–1450 MHz. It is a prime focus uncooled receiver with a characteristic system temperature of ~ 70 K. The 21 cm system has four sub-bands, centered at 1060, 1170, 1280 and 1390 MHz respectively, each with a 3 dB bandwidth of 120 MHz. At the time when these observations were carried out, this telescope was equipped with an FX correlator providing 128 channels per polarization per baseline. A baseband bandwidth ranging from 16 MHz down to 64 kHz variable in steps of 2 can be chosen.

4. Source selection

In selecting the sources, we have used a lower cutoff in flux density of 1 Jy at 20 cm wavelength. This was to ensure that we reach an rms in HI optical depth ~ 0.003

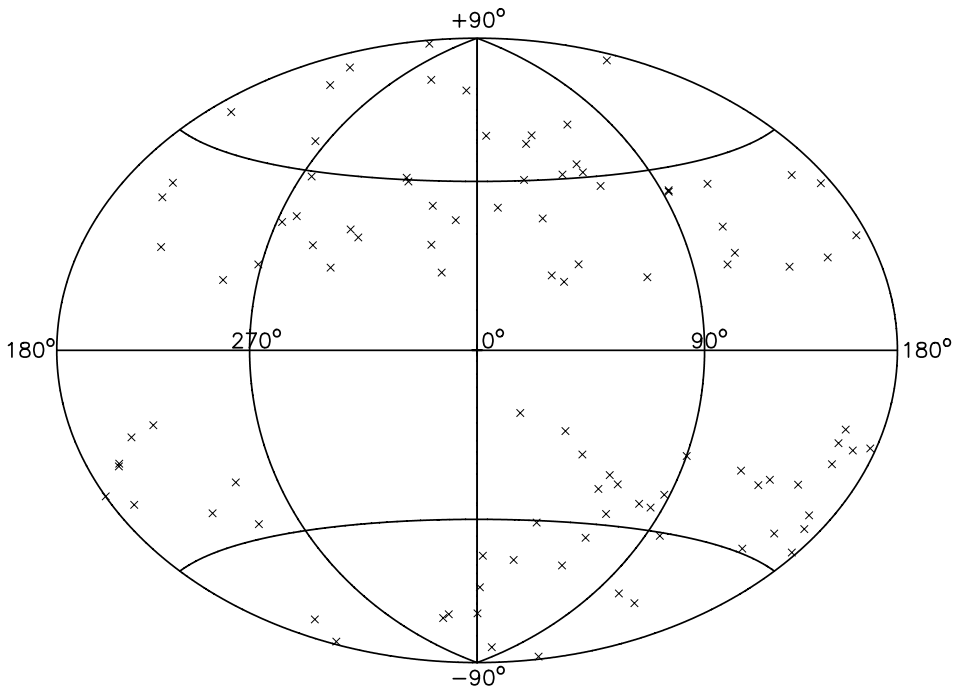

Figure 1. The distribution of program sources in Galactic co-ordinates. The fourth Galactic quadrant ($270^\circ < l < 360^\circ$) is not fully accessible for the GMRT, since this region is mainly in the southern equatorial hemisphere.

within an observing time $\lesssim 1$ h. In order to obtain a sample of these bright sources uniformly distributed all over the sky we used the VLA calibrator manual as the basic finding list. A list of 102 point sources, unresolved in the VLA B array configuration, with their Galactic latitude $|b| \geq 15^\circ$ were selected. Figure 1 shows the distribution of the program sources in the sky. The list of sources is given in Appendix A.

To supplement the absorption spectra, HI emission profiles were extracted from the Leiden–Dwingeloo all sky survey of Galactic neutral hydrogen (LDS, Hartmann & Burton 1995). This survey used the 25 meter Dwingeloo telescope to map the sky in HI emission. The full width at half maximum of the primary beam of the Dwingeloo telescope is $\sim 36'$. The geographic latitude of the Dwingeloo telescope is $\sim +53^\circ$ and that of the GMRT is $\sim +19^\circ$. Therefore some of the lines of sight in the southern hemisphere observed with the GMRT are not accessible to the Dwingeloo telescope.

5. Observations

The HI absorption observations were carried out using the GMRT during March–April 2000, and April–June 2001. On an average, we used ~ 20 antennas in the final analysis, though the actual number varied from 12 to 25. We used a baseband of width 2 MHz, which translates to ≈ 422 km s^{-1} in velocity and a resolution of ~ 3.3 km s^{-1}. The centre of the band was set at 1420.4 MHz. We used one of the VLA primary flux density calibrators (3C48/3C147/3C286) for setting the flux density scale. Since all the

Table 1. The Observational Setup.

Telescope	GMRT
System temperature	~ 70 K
Aperture efficiency	$\sim 40\%$
Baseband bandwidth	2.0 MHz
Number of channels	128
Velocity resolution	3.3 km s^{-1}
On source integration time	$\sim$ 10 to 60 minutes
rms noise (1 hr integration time)	~ 2 mJy beam^{-1} channel^{-1}

program sources were unresolved by the GMRT, they also served as phase calibrators. Bandpass calibration was carried out once every two hours for 10 minutes using 3C286, towards which no HI absorption was detected down to an rms in optical depth of $\tau_{\rm HI} \sim 0.002$. On source integration time ranged from 10 to 60 minutes, depending on its strength. The rms sensitivity in optical depth varied from 0.002 to 0.008 towards different sources, with a mean value ~ 0.003. A summary of the observational setup is given in Table 1.

6. Data analysis

The data were analysed using the Astronomical Image Processing System (AIPS) developed by the National Radio Astronomy Observatory. The observing band was found to be free from any kind of interference. The resulting data set consisted of 102 image cubes. The full width at half maximum of the synthesized beam width was in the range $\sim 6''$ to $\sim 25''$, depending on the number and locations of available antennas. Continuum subtraction was carried out by fitting a second order baseline to the line-free channels in the visibility domain and subtracting the best fit continuum from all the channels. Such a second order fit to the spectral baseline can result in the removal of broad and shallow absorption features. From the nature of the baselines fitted to the present dataset, we infer that any spectral features with FWHM $\gtrsim 50$ km s^{-1} and $\tau_{\rm HI} \lesssim 0.03$ would not be detected. However, the main aim of the present survey is to study the narrow absorption lines arising from the diffuse features in the CNM and the FWHM of such features are usually $\lesssim 10$ km s^{-1}. The second order fit also helps to achieve a better spectral dynamic range over the 2 MHz bandwidth. The resulting spectral dynamic range was ~ 500. However, for a few lines of sight, the bandpass errors were much larger and only a limited part of the observing band was found to be usable. To study the individual HI absorption components multiple Gaussian profiles were fitted to the absorption line spectra using the Groningen Image Processing System (GIPSY).

For an optically thin HI gas, the radiative transfer equation has a solution of the form (Spitzer 1978)

$$T_B = T_S(1 - e^{-\tau}), \tag{1}$$

where T_B is the brightness temperature, T_S is the spin (excitation) temperature and τ is the optical depth of the HI 21-cm line. Hence, knowing the line brightness temperature

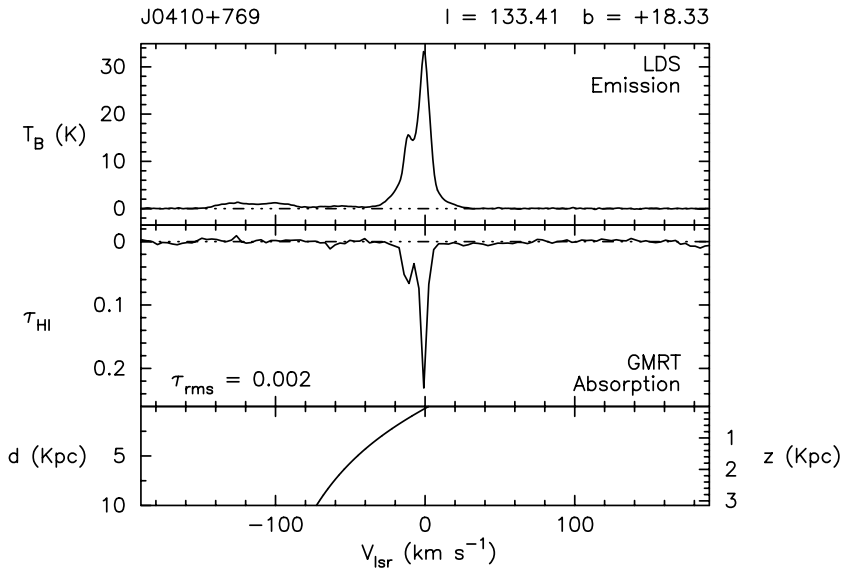

Figure 2. The HI optical depth spectrum from the GMRT towards one of the 102 sources (middle panel) and the corresponding HI brightness temperature profile from the Leiden–Dwingeloo survey (top panel). The lower panel is the Galactic rotation curve for the given line of sight obtained from the Galactic rotation model (Brand & Blitz 1993). The heliocentric distance as a function of radial velocity is labeled on the left of the lower panel and the corresponding height above the mid-plane of the Galaxy is labeled on the right side.

T_B, which is obtained from the HI emission profiles, and the optical depth τ, obtained from HI absorption, one can estimate the spin temperature T_S of HI gas.

Apart from the new HI absorption measurements with the GMRT, we have extracted the HI emission profiles towards these lines of sight (if available) from the Leiden–Dwingeloo sky survey (Hartmann & Burton 1995). We have used Gaussian fitting to the spectra to separate the profiles into discrete components. The HI emission profiles were Hanning smoothed over two channels, with a resulting velocity resolution of $\sim 2\,\mathrm{km\ s^{-1}}$. It is well known that the HI emission features are broader than the corresponding absorption features. This difference in the velocity width usually range from 0–5 km $\mathrm{s^{-1}}$ (Radhakrishnan *et al*. 1972b). It is also known that the wider HI emission features (FWHM $> 20\,\mathrm{km\ s^{-1}}$) arise in the warm neutral medium (WNM) (Radhakrishnan *et al*. 1972b). To identify the HI emission and absorption lines that arise from the same cloud, we have adopted the following considerations:

- The central velocities of the HI emission and absorption features are within the channel width, $\sim 3.3\,\mathrm{km\ s^{-1}}$, of the GMRT observations, and
- The difference between the widths of emission and the corresponding absorption line is less than $\sim 5\,\mathrm{km\ s^{-1}}$.

If both the above conditions were satisfied, we assume the features to arise from the same cloud. The second criterion excludes those instances where the velocity of a CNM absorption line match that of a WNM emission component. We have used the fitted values of τ and T_B to calculate the spin temperatures of HI features which are identified in both HI emission and absorption profiles. In those cases, where no HI absorption

feature was detected from our survey corresponding to the HI emission feature in the LDS survey data, we have estimated the lower limit for the spin temperature of the gas.

7. The spectra

Figure 2 is a sample spectrum of HI optical depth and the corresponding HI emission profile. In the figure, the lower panel is the Galactic rotation curve for the given line of sight obtained from the Galactic rotation model by Brand & Blitz (1993). We have used $R_0 = 8.5$ Kpc as the Galacto-centric distance and $\Theta_0 = 220\,\mathrm{km\ s^{-1}}$ as the solar orbital velocity around the Galactic centre. The rest of the spectra are given in Appendix B and the summary of the Gaussian fitting results are given in Appendix C. In all we have obtained 126 spectral components in HI absorption from GMRT and 478 components in HI emission from the LDS survey. The fitted parameters for the discrete components in HI absorption and emission were used to estimate the spin temperature of the respective features. A detailed analysis and interpretation of these spectra are given in an accompanying paper (Mohan *et al*. 2004; this volume).

Acknowledgements

We wish to thank C. R. Subrahmanya for useful discussions related to the GMRT offline software. We thank the referee, Miller Goss, for detailed comments and constructive criticism resulting in an improved version of this paper. We thank the staff of the GMRT who made these observations possible. The GMRT is operated by the National Centre for Radio Astrophysics of the Tata Institute of Fundamental Research. This research has made use of NASA's Astrophysics Data System.

Appendix A: The source list

The list of sources observed with the GMRT. The sixth column gives the rms optical depth in the HI absorption spectra and the last column lists the observed flux densities of the respective sources.

Source	α(J2000) (h m s)	δ(J2000) (° ′ ″)	l (°)	b (°)	τ_{rms}	S (Jy)
J0010 − 418	00 10 52.52	−41 53 10.8	329.68	−73.07	0.002	4.55
J0022 + 002	00 22 25.43	+00 14 56.1	107.46	−61.75	0.003	3.11
J0024 − 420	00 24 42.99	−42 02 04.0	321.35	−74.12	0.003	2.17
J0025 − 260	00 25 49.17	−26 02 12.7	42.27	−84.17	0.003	7.12
J0029 + 349	00 29 14.24	+34 56 32.2	117.79	−27.71	0.002	2.03
J0059 + 001	00 59 05.51	+00 06 51.6	127.11	−62.70	0.004	2.64
J0116 − 208	01 16 51.40	−20 52 06.8	167.11	−81.47	0.003	3.91
J0119 + 321	01 19 35.00	+32 10 50.1	129.83	−30.31	0.003	3.12
J0137 + 331	01 37 41.30	+33 09 35.1	133.96	−28.72	0.003	15.9
J0204 + 152	02 04 50.41	+15 14 11.0	147.93	−44.04	0.003	3.96
J0204 − 170	02 04 57.67	−17 01 19.8	185.99	−70.23	0.003	1.19
J0237 + 288	02 37 52.41	+28 48 09.0	149.47	−28.53	0.003	2.10
J0238 + 166	02 38 38.93	+16 36 59.3	156.77	−39.11	0.004	1.05
J0240 − 231	02 40 08.17	−23 09 15.7	209.79	−65.13	0.003	5.50

Source	α(J2000) (h m s)	δ(J2000) (○ ′ ″)	l (○)	b (○)	τ_{rms}	S (Jy)
J0318 + 164	03 18 57.80	+16 28 32.7	166.64	−33.60	0.002	8.65
J0321 + 123	03 21 53.10	+12 21 14.0	170.59	−36.24	0.002	2.07
J0323 + 055	03 23 20.26	+05 34 11.9	176.98	−40.84	0.003	3.04
J0329 + 279	03 29 57.67	+27 56 15.5	160.70	−23.07	0.003	1.40
J0336 + 323	03 36 30.11	+32 18 29.3	159.00	−18.77	0.004	2.71
J0348 + 338	03 48 46.90	+33 53 15.0	160.04	−15.91	0.003	2.32
J0403 + 260	04 03 05.59	+26 00 01.5	168.03	−19.65	0.004	1.08
J0409 + 122	04 09 22.01	+12 17 39.8	180.12	−27.90	0.003	1.46
J0410 + 769	04 10 45.61	+76 56 45.3	133.41	+18.33	0.002	5.70
J0424 + 020	04 24 08.56	+02 04 24.9	192.04	−31.10	0.004	1.33
J0431 + 206	04 31 03.76	+20 37 34.3	176.81	−18.56	0.003	3.40
J0440 − 435	04 40 17.18	−43 33 08.6	248.41	−41.57	0.003	3.28
J0453 − 281	04 53 14.65	−28 07 37.3	229.09	−37.02	0.004	2.18
J0459 + 024	04 59 52.05	+02 29 31.2	197.01	−23.34	0.003	1.93
J0503 + 020	05 3 21.20	+02 03 04.7	197.91	−22.82	0.004	2.26
J0538 − 440	05 38 50.36	−44 05 08.9	250.08	−31.09	0.002	2.75
J0541 − 056	05 41 38.08	−05 41 49.4	210.05	−18.11	0.004	1.42
J0609 − 157	06 09 40.95	−15 42 40.7	222.61	−16.18	0.007	2.78
J0614 + 607	06 14 23.87	+60 46 21.8	153.60	+19.15	0.005	1.17
J0713 + 438	07 13 38.16	+43 49 17.2	173.79	+22.20	0.004	2.33
J0814 + 459	08 14 30.31	+45 56 39.5	173.90	+33.17	0.005	1.13
J0825 + 031	08 25 50.34	+03 09 24.5	221.22	+22.39	0.002	1.12
J0834 + 555	08 34 54.90	+55 34 21.1	162.23	+36.56	0.002	9.15
J0842 + 185	08 42 05.09	+18 35 41.0	207.28	+32.48	0.004	1.17
J0854 + 201	08 54 48.87	+20 06 30.6	206.81	+35.82	0.002	1.65
J0921 − 263	09 21 29.35	−26 18 43.4	255.07	+16.48	0.003	1.41
J0958 + 324	09 58 20.95	+32 24 02.2	194.17	+52.32	0.005	1.47
J1018 − 317	10 18 09.28	−31 44 14.1	268.61	+20.73	0.002	3.44
J1057 − 245	10 57 55.42	−24 33 48.9	272.47	+31.51	0.004	1.10
J1111 + 199	11 11 20.07	+19 55 36.0	225.01	+66.00	0.003	1.52
J1119 − 030	11 19 25.30	−03 02 51.3	263.01	+52.54	0.002	1.44
J1120 − 251	11 20 09.12	−25 08 07.6	278.09	+33.30	0.003	1.31
J1125 + 261	11 25 53.71	+26 10 20.0	210.92	+70.89	0.003	0.96
J1130 − 148	11 30 07.05	−14 49 27.4	275.28	+43.64	0.002	5.96
J1146 + 399	11 46 58.30	+39 58 34.3	164.95	+71.47	0.009	0.47
J1154 − 350	11 54 21.79	−35 05 29.0	289.93	+26.34	0.002	5.48
J1221 + 282	12 21 31.69	+28 13 58.5	201.74	+83.29	0.004	1.03
J1235 − 418	12 35 41.93	−41 53 18.0	299.80	+20.89	0.003	1.57
J1254 + 116	12 54 38.26	+11 41 05.9	305.87	+74.54	0.005	0.93
J1257 − 319	12 57 59.06	−31 55 16.9	304.55	+30.93	0.003	1.21
J1316 − 336	13 16 07.99	−33 38 59.2	308.80	+28.94	0.006	1.11
J1344 + 141	13 44 23.74	+14 09 14.9	349.16	+72.09	0.003	1.34
J1351 − 148	13 51 52.65	−14 49 14.9	324.03	+45.56	0.003	1.16

Source	α(J2000) (h m s)	δ(J2000) (° ′ ″)	l (°)	b (°)	τ_{rms}	S (Jy)
J1357 − 154	13 57 11.24	−15 27 28.8	325.42	+44.52	0.015	1.11
J1435 + 760	14 35 47.10	+76 05 25.8	115.07	+39.40	0.003	1.19
J1445 + 099	14 45 16.47	+09 58 36.1	5.79	+58.17	0.002	2.62
J1448 − 163	14 48 15.05	−16 20 24.5	339.45	+38.11	0.003	1.63
J1506 + 375	15 06 09.53	+37 30 51.1	61.65	+59.90	0.003	1.15
J1513 + 236	15 13 40.19	+23 38 35.2	34.77	+57.79	0.002	1.73
J1517 − 243	15 17 41.81	−24 22 19.5	340.68	+27.58	0.004	2.53
J1520 + 202	15 20 05.49	+20 16 05.6	29.64	+55.42	0.003	3.17
J1526 − 138	15 26 59.44	−13 51 00.1	350.48	+34.29	0.002	2.63
J1553 + 129	15 53 32.70	+12 56 51.7	23.79	+45.22	0.003	1.49
J1554 − 270	15 54 02.49	−27 04 40.2	345.68	+20.27	0.003	1.52
J1557 − 000	15 57 51.43	+00 01 50.4	9.58	+37.68	0.004	0.95
J1602 + 334	16 02 07.26	+33 26 53.1	53.73	+48.71	0.002	3.33
J1609 + 266	16 09 13.32	+26 41 29.0	44.17	+46.20	0.003	4.57
J1613 + 342	16 13 41.06	+34 12 47.9	55.15	+46.38	0.001	5.35
J1634 + 627	16 34 33.80	+62 45 35.9	93.61	+39.38	0.002	4.67
J1635 + 381	16 35 15.49	+38 08 04.5	61.09	+42.34	0.002	3.45
J1638 + 625	16 38 28.21	+62 34 44.3	93.22	+39.01	0.003	4.65
J1640 + 123	16 40 47.93	+12 20 02.1	29.43	+34.51	0.003	1.87
J1737 + 063	17 37 13.73	+06 21 03.5	30.15	+19.38	0.005	0.87
J1745 + 173	17 45 35.21	+17 20 01.4	41.74	+22.12	0.004	1.19
J1751 + 096	17 51 32.82	+09 39 00.7	34.92	+17.65	0.002	1.76
J1800 + 784	18 00 45.68	+78 28 04.1	110.04	+29.07	0.002	2.71
J1845 + 401	18 45 11.12	+40 07 51.5	69.36	+18.21	0.003	1.41
J1923 − 210	19 23 32.19	−21 04 33.3	17.18	−16.25	0.003	2.82
J2005 + 778	20 05 31.00	+77 52 43.2	110.46	+22.73	0.003	1.38
J2009 + 724	20 09 52.30	+72 29 19.4	105.36	+20.18	0.003	1.00
J2011 − 067	20 11 14.22	−06 44 03.6	36.01	−20.80	0.002	3.39
J2047 − 026	20 47 10.35	−02 36 22.2	44.56	−26.80	0.002	2.94
J2130 + 050	21 30 32.88	+05 02 17.5	58.65	−31.81	0.002	5.05
J2136 + 006	21 36 38.59	+00 41 54.2	55.47	−35.58	0.002	5.22
J2137 − 207	21 37 50.00	−20 42 31.8	30.35	−45.56	0.002	3.87
J2148 + 069	21 48 05.46	+06 57 38.6	63.66	−34.07	0.002	3.74
J2212 + 018	22 12 37.98	+01 52 51.2	63.68	−42.02	0.001	3.95
J2214 − 385	22 14 38.57	−38 35 45.0	3.47	−55.44	0.002	1.76
J2219 − 279	22 19 40.94	−27 56 26.9	22.57	−56.48	0.003	2.55
J2225 − 049	22 25 47.26	−04 57 01.4	58.96	−48.84	0.003	5.32
J2232 + 117	22 32 36.41	+11 43 50.9	77.44	−38.58	0.003	7.43
J2236 + 284	22 36 22.47	+28 28 57.4	90.12	−25.65	0.004	1.38
J2246 − 121	22 46 18.23	−12 06 51.3	53.87	−57.07	0.003	2.26
J2250 + 143	22 50 25.54	+14 19 50.6	83.89	−39.20	0.002	2.16
J2251 + 188	22 51 34.74	+18 48 40.1	87.35	−35.65	0.002	3.24
J2302 − 373	23 02 23.89	−37 18 06.8	2.16	−64.91	0.002	3.09
J2340 + 135	23 40 33.22	+13 33 00.9	97.80	−45.83	0.002	2.82
J2341 − 351	23 41 45.89	−35 06 22.1	0.45	−73.12	0.004	2.06

Appendix B: The spectra

In this Appendix, we present the HI optical depth profiles obtained from the high latitude Galactic HI absorption survey using the GMRT along with the HI emission profiles in the respective lines of sight from the Leiden–Dwingeloo survey of Galactic neutral hydrogen (if available). The figures are arranged in order of increasing right ascension. The spectra are labeled by the radio continuum source name in J2000.0 co-ordinates (top left) and its Galactic co-ordinates (top right).

For each of the figures, the HI emission profile from the Leiden–Dwingeloo survey is shown in the top panel and the HI optical depth profile from the GMRT is shown in the middle panel. The lower panel is the Galactic rotation curve for the given line of sight. The heliocentric distance as a function of radial velocity ($V_{\rm lsr}$) is labeled on the left of this panel and the corresponding height above the mid-plane of the Galaxy is labeled on its right side. For a few lines of sight, only the reliable part of the observing band is shown.

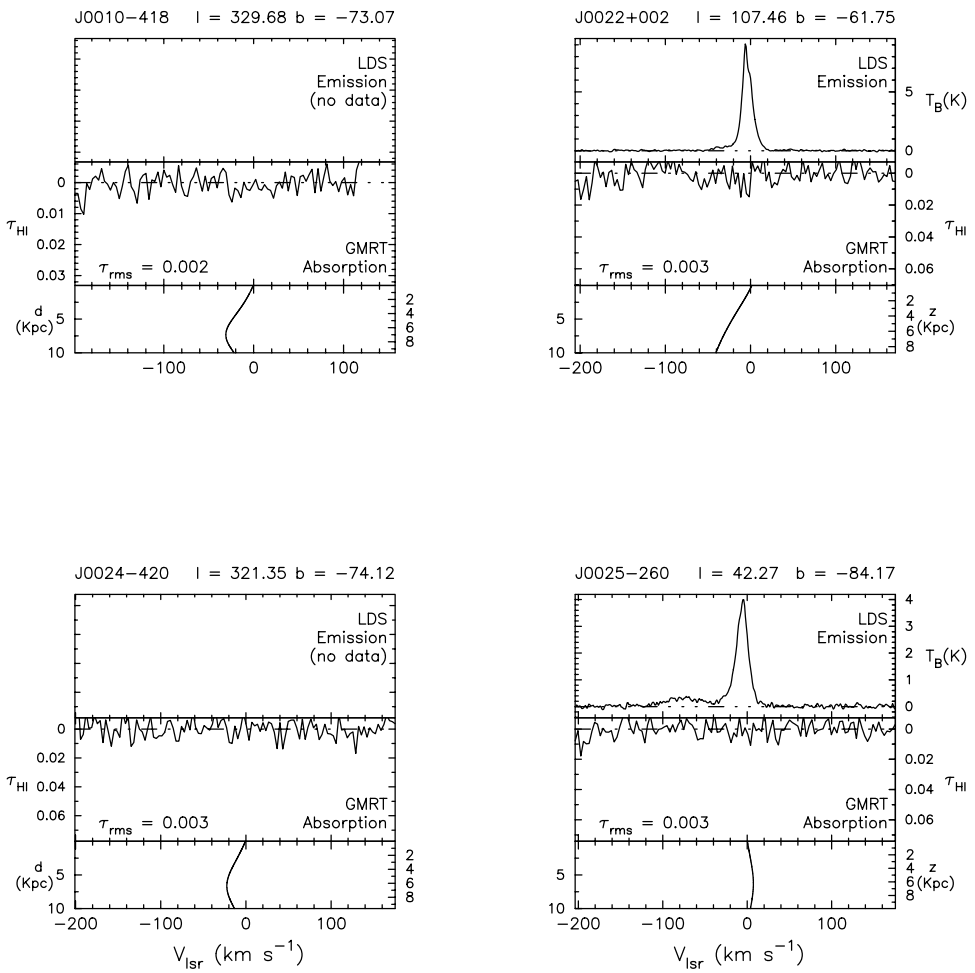

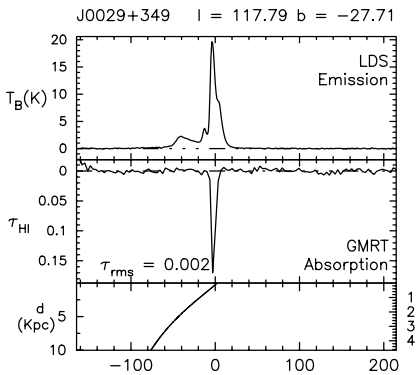
J0029+349 l = 117.79 b = −27.71
LDS
Emission
T_B(K)
GMRT
Absorption
τ_{rms} = 0.002
τ_{HI}
d (Kpc)

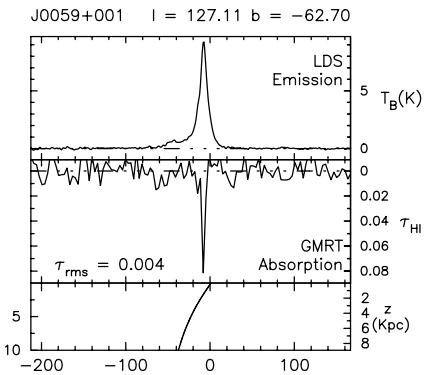
J0059+001 l = 127.11 b = −62.70
LDS
Emission
T_B(K)
GMRT
Absorption
τ_{rms} = 0.004
τ_{HI}
z (Kpc)

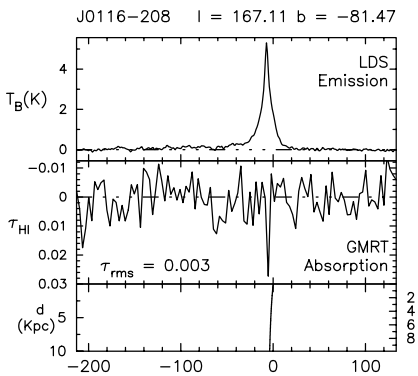
J0116−208 l = 167.11 b = −81.47
LDS
Emission
T_B(K)
GMRT
Absorption
τ_{rms} = 0.003
τ_{HI}
d (Kpc)

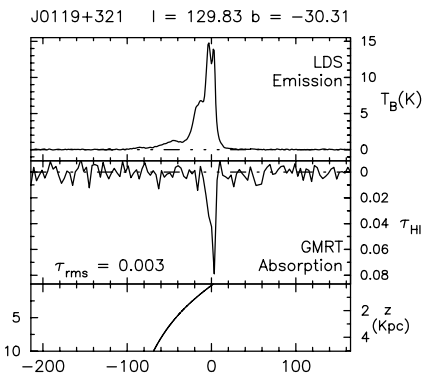
J0119+321 l = 129.83 b = −30.31
LDS
Emission
T_B(K)
GMRT
Absorption
τ_{rms} = 0.003
τ_{HI}
z (Kpc)

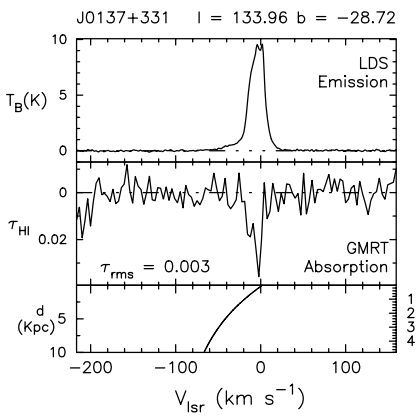
J0137+331 l = 133.96 b = −28.72
LDS
Emission
T_B(K)
GMRT
Absorption
τ_{rms} = 0.003
τ_{HI}
d (Kpc)
V_{lsr} (km s^{-1})

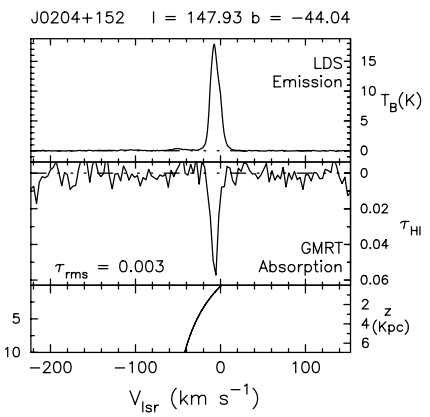
J0204+152 l = 147.93 b = −44.04
LDS
Emission
T_B(K)
GMRT
Absorption
τ_{rms} = 0.003
τ_{HI}
z (Kpc)
V_{lsr} (km s^{-1})

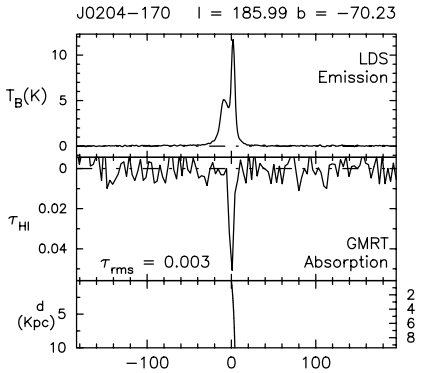
J0204−170 l = 185.99 b = −70.23
LDS
Emission
GMRT
Absorption
τ_{rms} = 0.003
T_B(K)
τ_{HI}
d (Kpc)

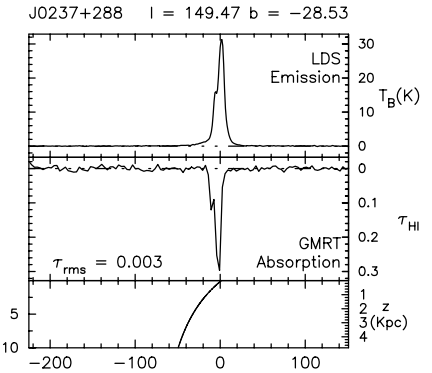
J0237+288 l = 149.47 b = −28.53
LDS
Emission
GMRT
Absorption
τ_{rms} = 0.003
T_B(K)
τ_{HI}
z (Kpc)

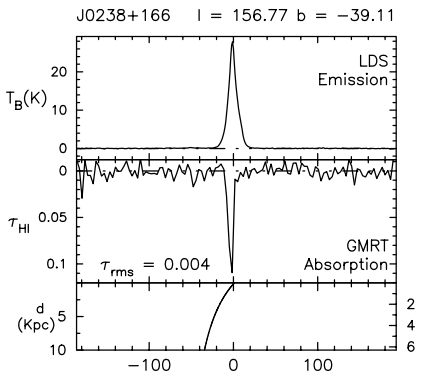
J0238+166 l = 156.77 b = −39.11
LDS
Emission
GMRT
Absorption
τ_{rms} = 0.004
T_B(K)
τ_{HI}
d (Kpc)

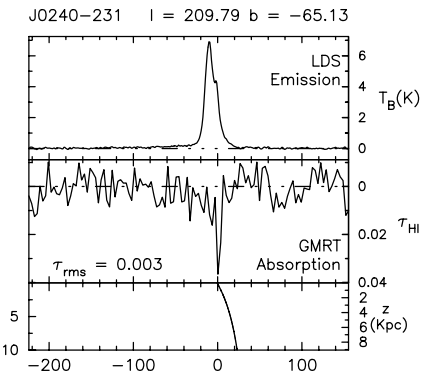
J0240−231 l = 209.79 b = −65.13
LDS
Emission
GMRT
Absorption
τ_{rms} = 0.003
T_B(K)
τ_{HI}
z (Kpc)

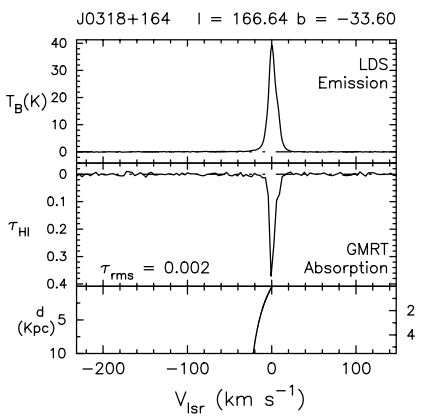
J0318+164 l = 166.64 b = −33.60
LDS
Emission
GMRT
Absorption
τ_{rms} = 0.002
T_B(K)
τ_{HI}
d (Kpc)
V_{lsr} (km s^{-1})

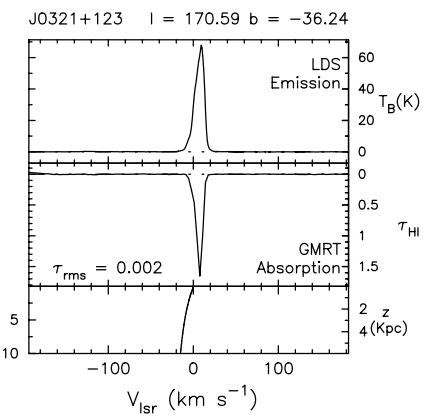
J0321+123 l = 170.59 b = −36.24
LDS
Emission
GMRT
Absorption
τ_{rms} = 0.002
T_B(K)
τ_{HI}
z (Kpc)
V_{lsr} (km s^{-1})

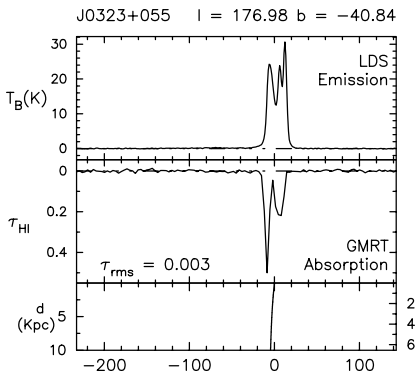
J0323+055 l = 176.98 b = −40.84
LDS
Emission
GMRT
Absorption
τrms = 0.003
TB(K)
τHI
d
(Kpc)

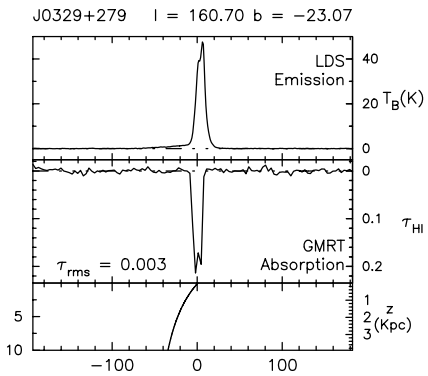
J0329+279 l = 160.70 b = −23.07
LDS
Emission
GMRT
Absorption
τrms = 0.003
TB(K)
τHI
z
(Kpc)

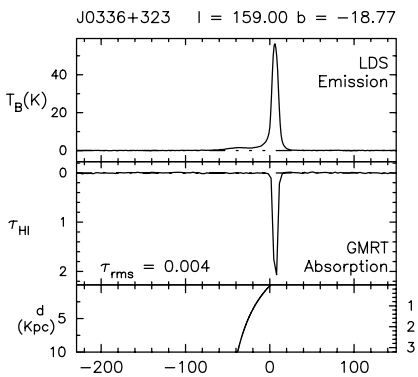
J0336+323 l = 159.00 b = −18.77
LDS
Emission
GMRT
Absorption
τrms = 0.004
TB(K)
τHI
d
(Kpc)

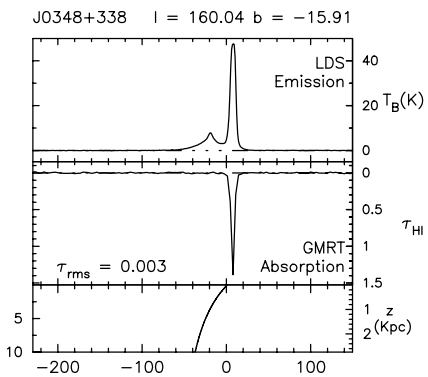
J0348+338 l = 160.04 b = −15.91
LDS
Emission
GMRT
Absorption
τrms = 0.003
TB(K)
τHI
z
(Kpc)

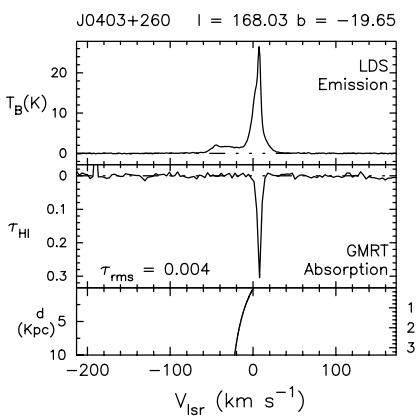
J0403+260 l = 168.03 b = −19.65
LDS
Emission
GMRT
Absorption
τrms = 0.004
TB(K)
τHI
d
(Kpc)
Vlsr (km s−1)

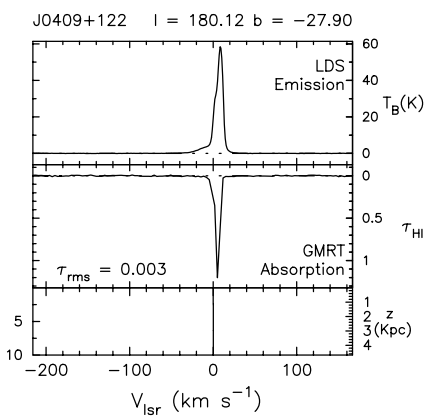
J0409+122 l = 180.12 b = −27.90
LDS
Emission
GMRT
Absorption
τrms = 0.003
TB(K)
τHI
z
(Kpc)
Vlsr (km s−1)

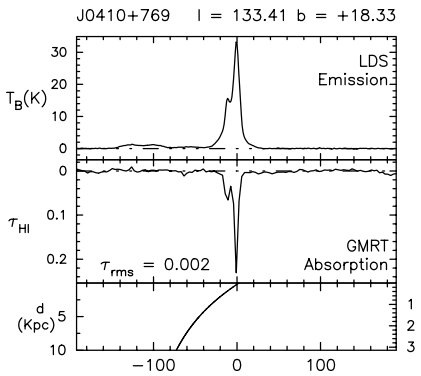
J0410+769 l = 133.41 b = +18.33
LDS
Emission
T_B(K)
GMRT
Absorption
τ_{rms} = 0.002
τ_{HI}
d
(Kpc)

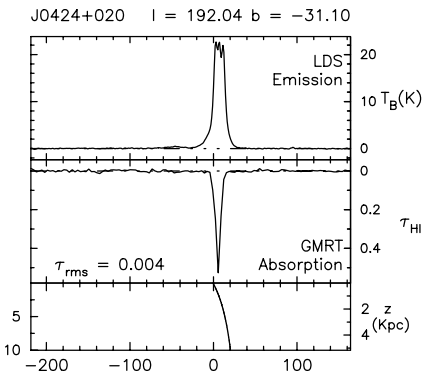
J0424+020 l = 192.04 b = −31.10
LDS
Emission
T_B(K)
GMRT
Absorption
τ_{rms} = 0.004
τ_{HI}
z
(Kpc)

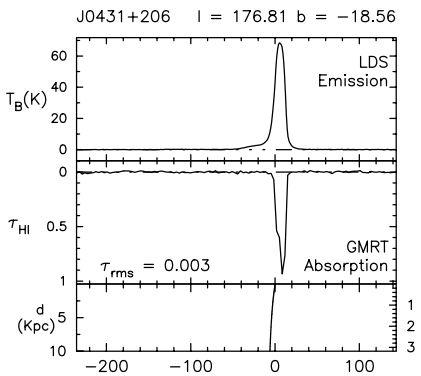
J0431+206 l = 176.81 b = −18.56
LDS
Emission
T_B(K)
GMRT
Absorption
τ_{rms} = 0.003
τ_{HI}
d
(Kpc)

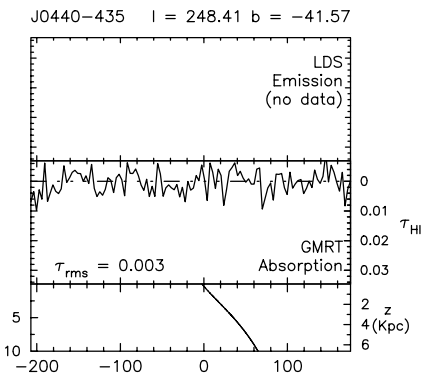
J0440−435 l = 248.41 b = −41.57
LDS
Emission
(no data)
GMRT
Absorption
τ_{rms} = 0.003
τ_{HI}
z
(Kpc)

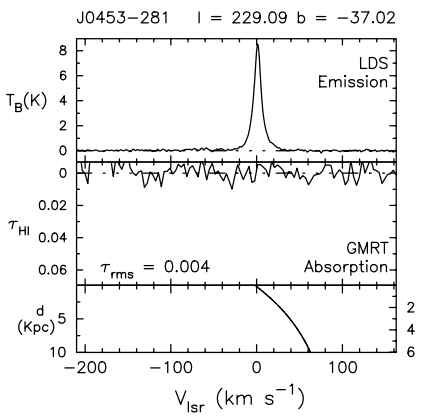
J0453−281 l = 229.09 b = −37.02
LDS
Emission
T_B(K)
GMRT
Absorption
τ_{rms} = 0.004
τ_{HI}
d
(Kpc)
V_{lsr} (km s^{-1})

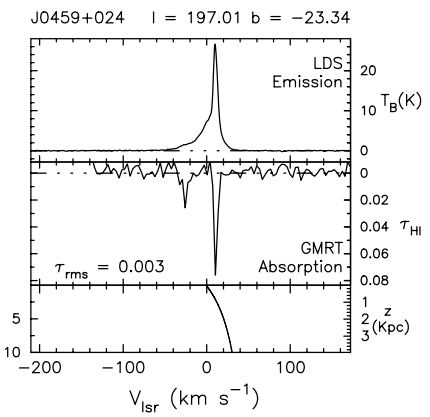
J0459+024 l = 197.01 b = −23.34
LDS
Emission
T_B(K)
GMRT
Absorption
τ_{rms} = 0.003
τ_{HI}
z
(Kpc)
V_{lsr} (km s^{-1})

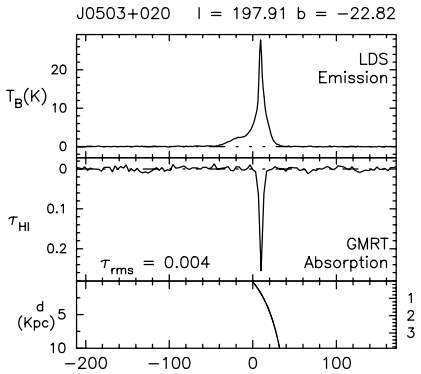
J0503+020 l = 197.91 b = −22.82
LDS
Emission
T_B(K)
τ_{HI}
GMRT
Absorption
τ_{rms} = 0.004
d (Kpc)

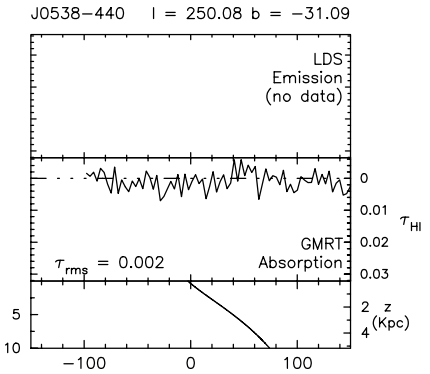
J0538−440 l = 250.08 b = −31.09
LDS
Emission
(no data)
τ_{HI}
GMRT
Absorption
τ_{rms} = 0.002
z (Kpc)

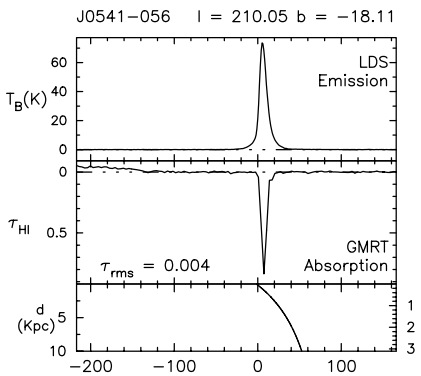
J0541−056 l = 210.05 b = −18.11
LDS
Emission
T_B(K)
τ_{HI}
GMRT
Absorption
τ_{rms} = 0.004
d (Kpc)

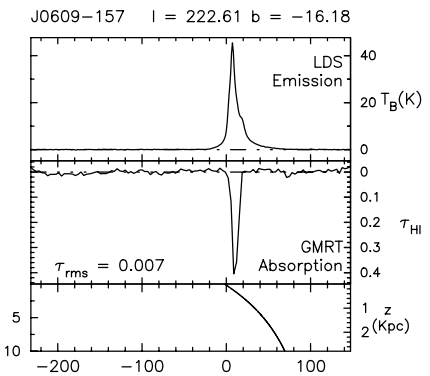
J0609−157 l = 222.61 b = −16.18
LDS
Emission
T_B(K)
τ_{HI}
GMRT
Absorption
τ_{rms} = 0.007
z (Kpc)

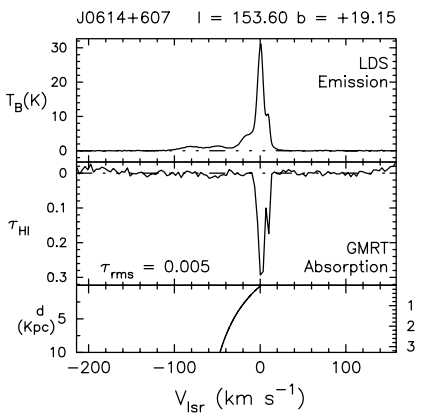
J0614+607 l = 153.60 b = +19.15
LDS
Emission
T_B(K)
τ_{HI}
GMRT
Absorption
τ_{rms} = 0.005
d (Kpc)
V_{lsr} (km s^{-1})

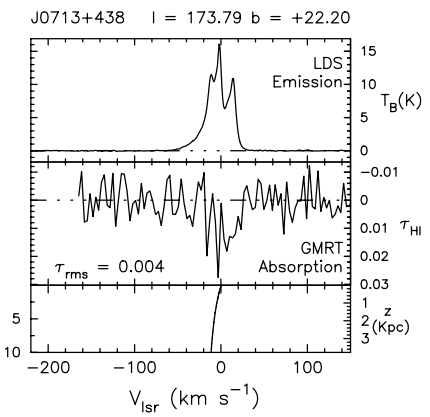
J0713+438 l = 173.79 b = +22.20
LDS
Emission
T_B(K)
τ_{HI}
GMRT
Absorption
τ_{rms} = 0.004
z (Kpc)
V_{lsr} (km s^{-1})

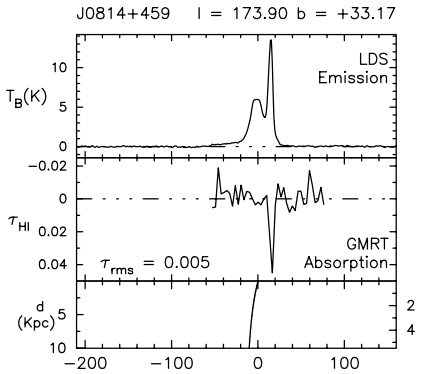
J0814+459 l = 173.90 b = +33.17
LDS
Emission
T_B(K)
GMRT
Absorption
τ_{rms} = 0.005
τ_{HI}
d
(Kpc)

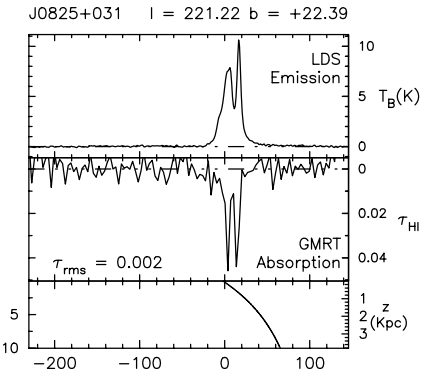
J0825+031 l = 221.22 b = +22.39
LDS
Emission
T_B(K)
GMRT
Absorption
τ_{rms} = 0.002
τ_{HI}
z
(Kpc)

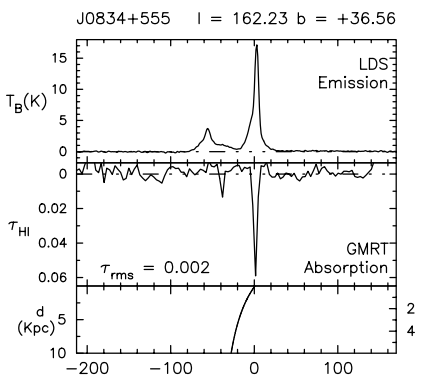
J0834+555 l = 162.23 b = +36.56
LDS
Emission
T_B(K)
GMRT
Absorption
τ_{rms} = 0.002
τ_{HI}
d
(Kpc)

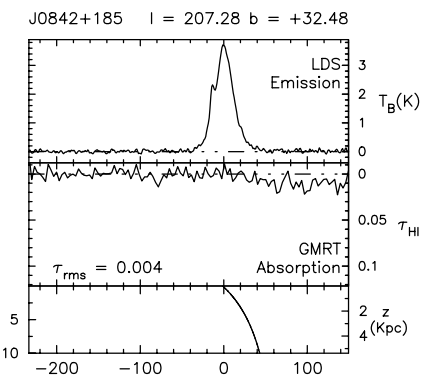
J0842+185 l = 207.28 b = +32.48
LDS
Emission
T_B(K)
GMRT
Absorption
τ_{rms} = 0.004
τ_{HI}
z
(Kpc)

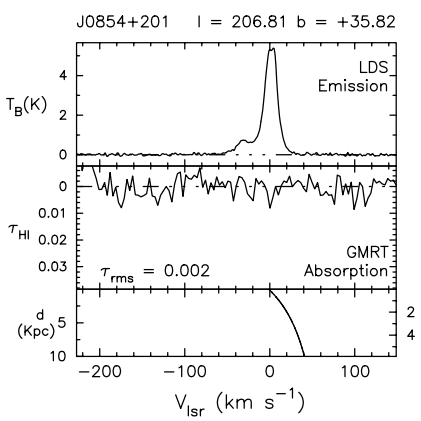
J0854+201 l = 206.81 b = +35.82
LDS
Emission
T_B(K)
GMRT
Absorption
τ_{rms} = 0.002
τ_{HI}
d
(Kpc)
V_{lsr} (km s^{-1})

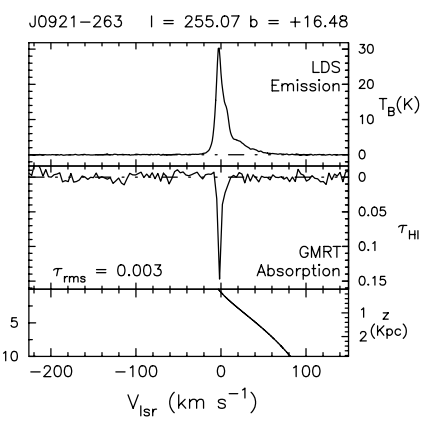
J0921−263 l = 255.07 b = +16.48
LDS
Emission
T_B(K)
GMRT
Absorption
τ_{rms} = 0.003
τ_{HI}
z
(Kpc)
V_{lsr} (km s^{-1})

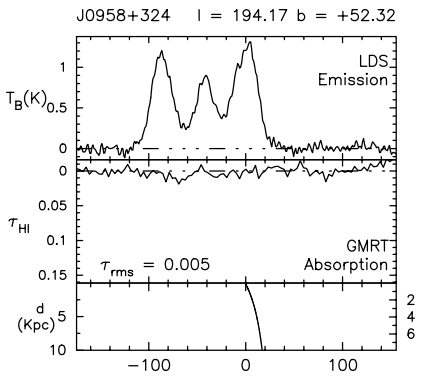
J0958+324 l = 194.17 b = +52.32
LDS
Emission
GMRT
Absorption
τ_{rms} = 0.005
T_B(K)
τ_{HI}
d (Kpc)

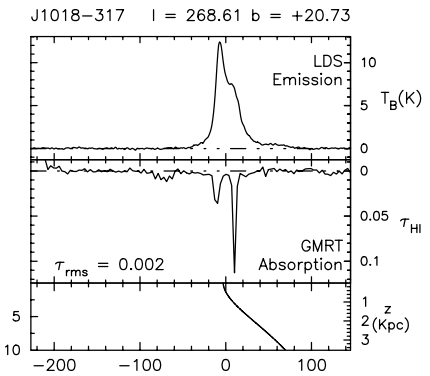
J1018−317 l = 268.61 b = +20.73
LDS
Emission
GMRT
Absorption
τ_{rms} = 0.002
T_B(K)
τ_{HI}
z (Kpc)

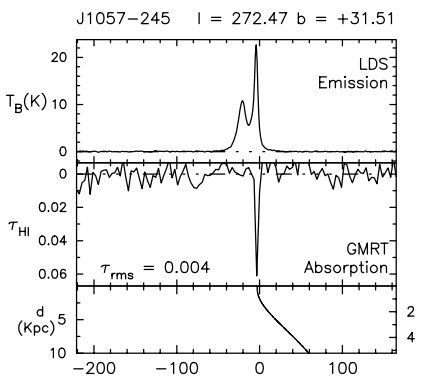
J1057−245 l = 272.47 b = +31.51
LDS
Emission
GMRT
Absorption
τ_{rms} = 0.004
T_B(K)
τ_{HI}
d (Kpc)

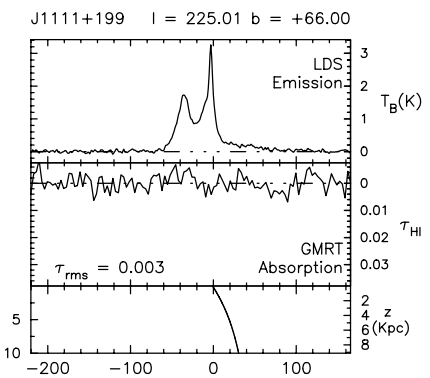
J1111+199 l = 225.01 b = +66.00
LDS
Emission
GMRT
Absorption
τ_{rms} = 0.003
T_B(K)
τ_{HI}
z (Kpc)

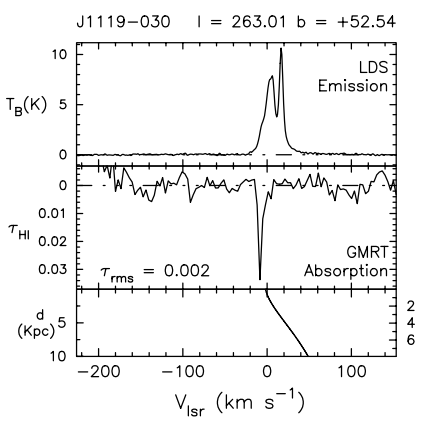
J1119−030 l = 263.01 b = +52.54
LDS
Emission
GMRT
Absorption
τ_{rms} = 0.002
T_B(K)
τ_{HI}
d (Kpc)
V_{lsr} (km s^{-1})

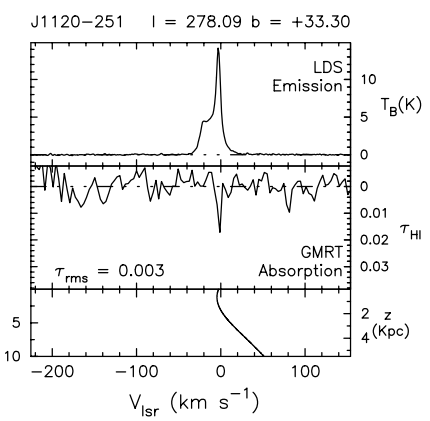
J1120−251 l = 278.09 b = +33.30
LDS
Emission
GMRT
Absorption
τ_{rms} = 0.003
T_B(K)
τ_{HI}
z (Kpc)
V_{lsr} (km s^{-1})

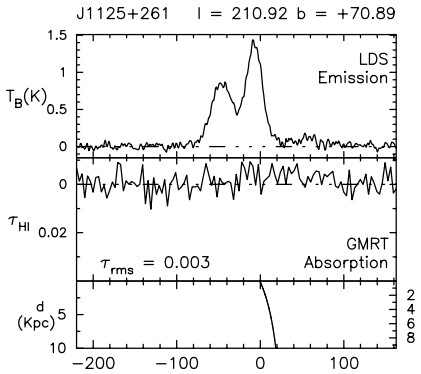
J1125+261 l = 210.92 b = +70.89
LDS
Emission
GMRT
Absorption
τ_{rms} = 0.003
T_B(K)
τ_{HI}
d (Kpc)

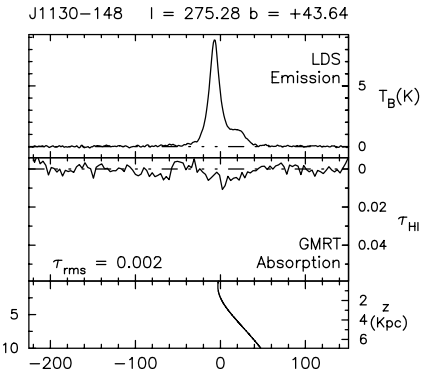
J1130−148 l = 275.28 b = +43.64
LDS
Emission
GMRT
Absorption
τ_{rms} = 0.002
T_B(K)
τ_{HI}
z (Kpc)

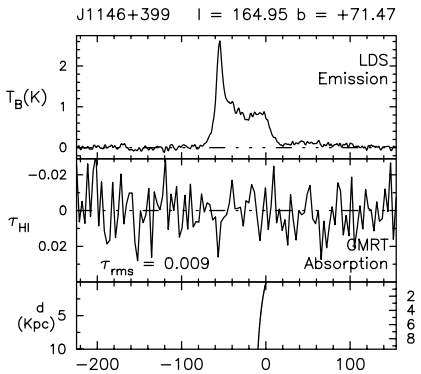
J1146+399 l = 164.95 b = +71.47
LDS
Emission
GMRT
Absorption
τ_{rms} = 0.009
T_B(K)
τ_{HI}
d (Kpc)

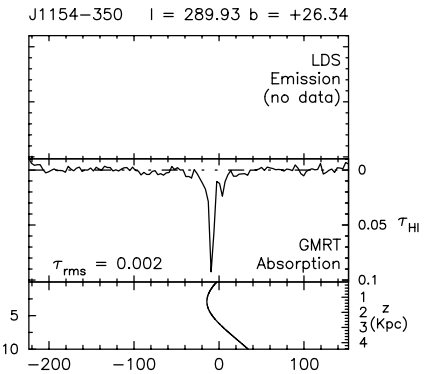
J1154−350 l = 289.93 b = +26.34
LDS
Emission
(no data)
GMRT
Absorption
τ_{rms} = 0.002
τ_{HI}
z (Kpc)

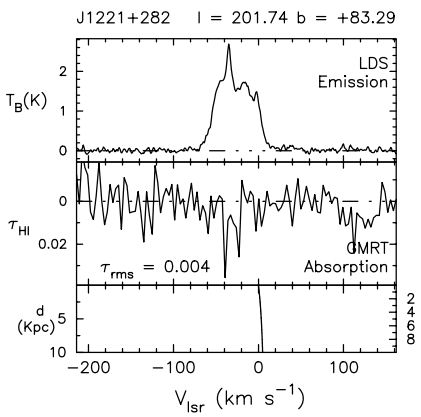
J1221+282 l = 201.74 b = +83.29
LDS
Emission
GMRT
Absorption
τ_{rms} = 0.004
T_B(K)
τ_{HI}
d (Kpc)
V_{lsr} (km s^{-1})

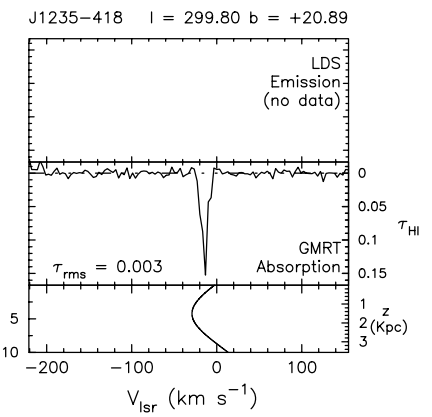
J1235−418 l = 299.80 b = +20.89
LDS
Emission
(no data)
GMRT
Absorption
τ_{rms} = 0.003
τ_{HI}
z (Kpc)
V_{lsr} (km s^{-1})

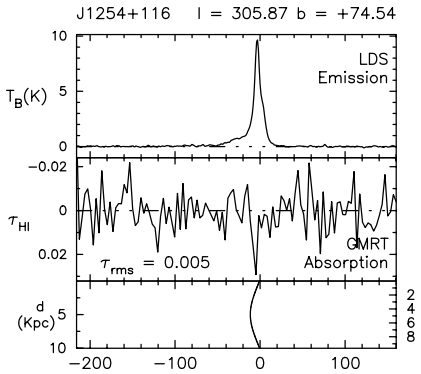
J1254+116 l = 305.87 b = +74.54
LDS
Emission
T_B(K)
GMRT
Absorption
τ_{rms} = 0.005
τ_{HI}
d (Kpc)
−200 −100 0 100

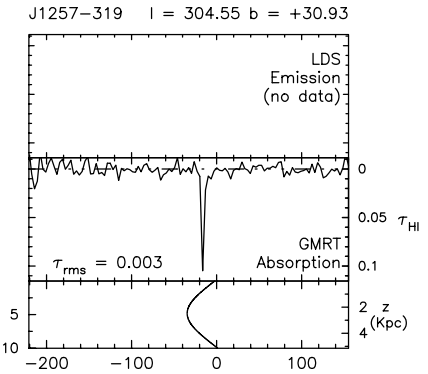
J1257−319 l = 304.55 b = +30.93
LDS
Emission
(no data)
GMRT
Absorption
τ_{rms} = 0.003
τ_{HI}
z (Kpc)
−200 −100 0 100

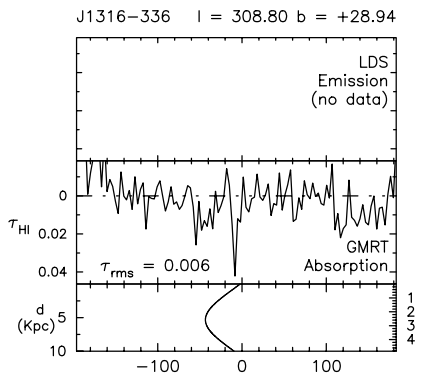
J1316−336 l = 308.80 b = +28.94
LDS
Emission
(no data)
GMRT
Absorption
τ_{rms} = 0.006
τ_{HI}
d (Kpc)
−100 0 100

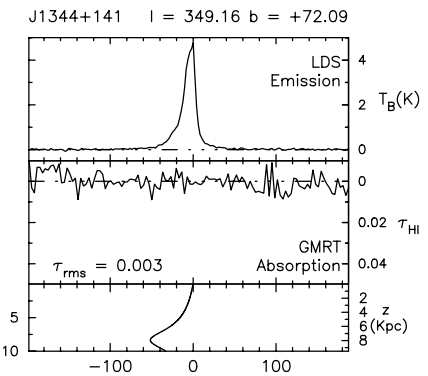
J1344+141 l = 349.16 b = +72.09
LDS
Emission
T_B(K)
GMRT
Absorption
τ_{rms} = 0.003
τ_{HI}
z (Kpc)
−100 0 100

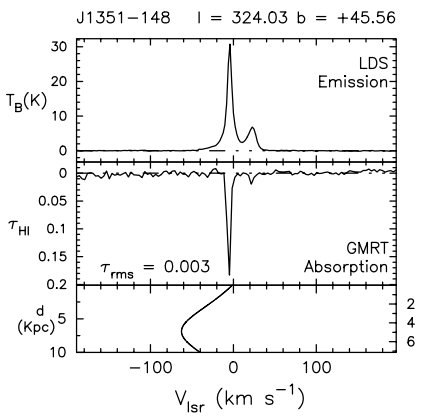
J1351−148 l = 324.03 b = +45.56
LDS
Emission
T_B(K)
GMRT
Absorption
τ_{rms} = 0.003
τ_{HI}
d (Kpc)
−100 0 100
V_{lsr} (km s^{-1})

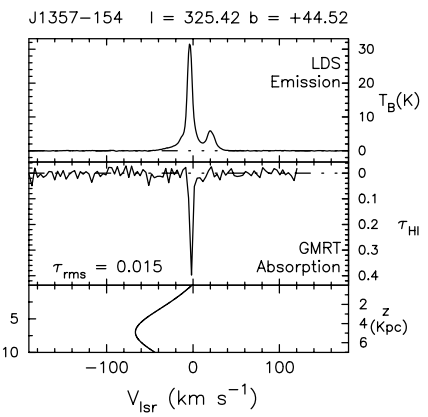
J1357−154 l = 325.42 b = +44.52
LDS
Emission
T_B(K)
GMRT
Absorption
τ_{rms} = 0.015
τ_{HI}
z (Kpc)
−100 0 100
V_{lsr} (km s^{-1})

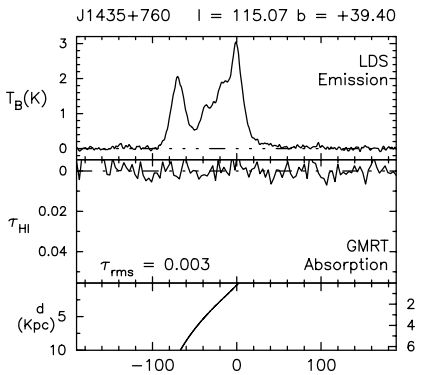
J1435+760 l = 115.07 b = +39.40
LDS
Emission
GMRT
Absorption
τ_{rms} = 0.003
T_B(K)
τ_{HI}
d (Kpc)

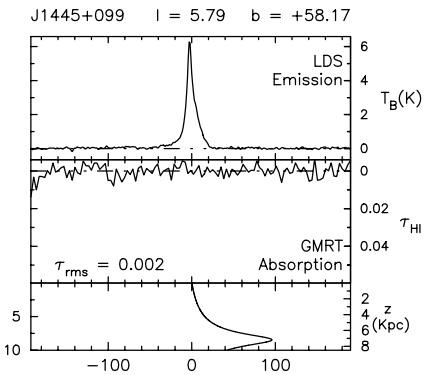
J1445+099 l = 5.79 b = +58.17
LDS
Emission
GMRT
Absorption
τ_{rms} = 0.002
T_B(K)
τ_{HI}
z (Kpc)

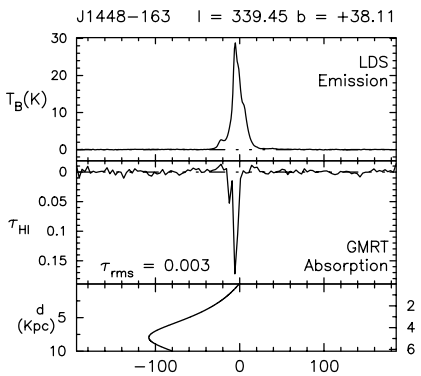
J1448−163 l = 339.45 b = +38.11
LDS
Emission
GMRT
Absorption
τ_{rms} = 0.003
T_B(K)
τ_{HI}
d (Kpc)

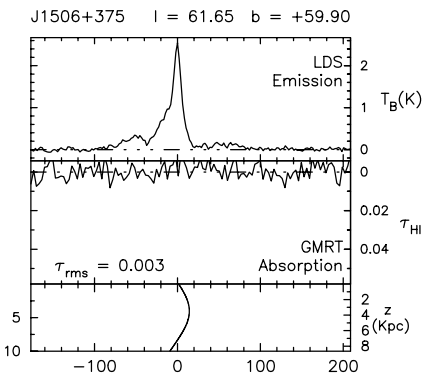
J1506+375 l = 61.65 b = +59.90
LDS
Emission
GMRT
Absorption
τ_{rms} = 0.003
T_B(K)
τ_{HI}
z (Kpc)

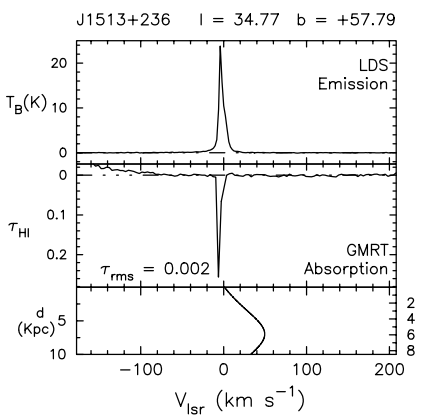
J1513+236 l = 34.77 b = +57.79
LDS
Emission
GMRT
Absorption
τ_{rms} = 0.002
T_B(K)
τ_{HI}
d (Kpc)
V_{lsr} (km s^{-1})

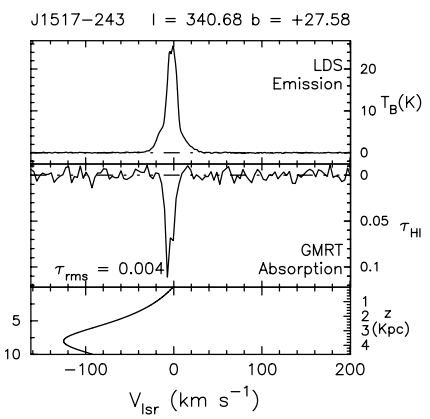
J1517−243 l = 340.68 b = +27.58
LDS
Emission
GMRT
Absorption
τ_{rms} = 0.004
T_B(K)
τ_{HI}
z (Kpc)
V_{lsr} (km s^{-1})

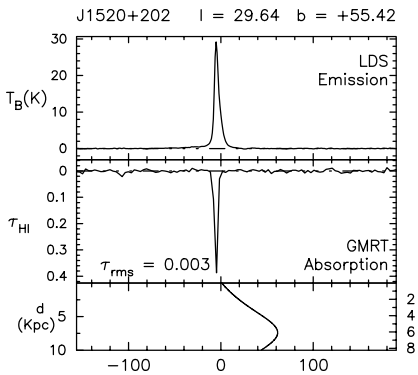
J1520+202 l = 29.64 b = +55.42
LDS
Emission
GMRT
Absorption
τ_{rms} = 0.003
T_B(K)
τ_{HI}
d (Kpc)

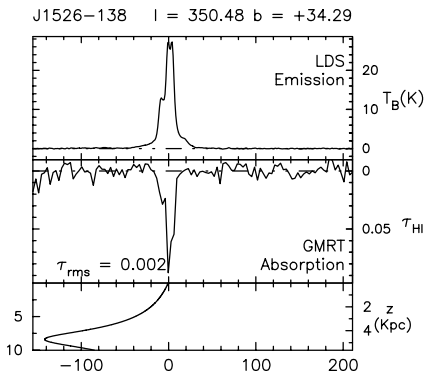
J1526−138 l = 350.48 b = +34.29
LDS
Emission
GMRT
Absorption
τ_{rms} = 0.002
T_B(K)
τ_{HI}
z (Kpc)

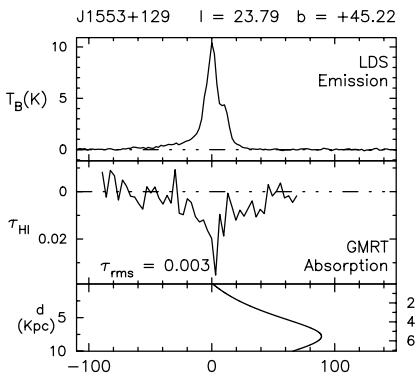
J1553+129 l = 23.79 b = +45.22
LDS
Emission
GMRT
Absorption
τ_{rms} = 0.003
T_B(K)
τ_{HI}
d (Kpc)

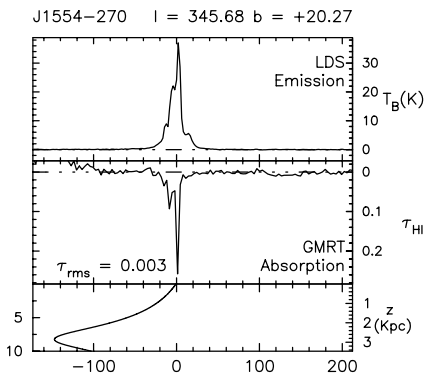
J1554−270 l = 345.68 b = +20.27
LDS
Emission
GMRT
Absorption
τ_{rms} = 0.003
T_B(K)
τ_{HI}
z (Kpc)

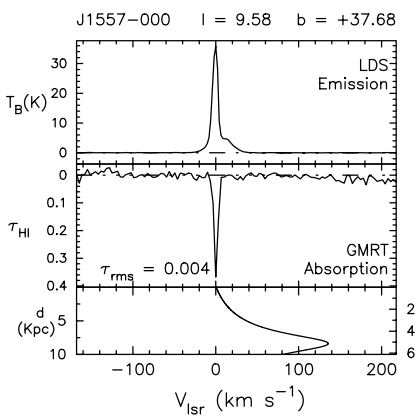
J1557−000 l = 9.58 b = +37.68
LDS
Emission
GMRT
Absorption
τ_{rms} = 0.004
T_B(K)
τ_{HI}
d (Kpc)
V_{lsr} (km s^{-1})

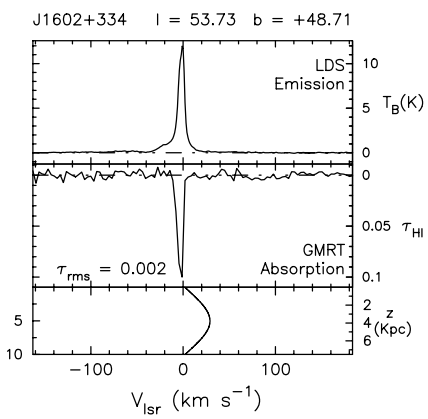
J1602+334 l = 53.73 b = +48.71
LDS
Emission
GMRT
Absorption
τ_{rms} = 0.002
T_B(K)
τ_{HI}
z (Kpc)
V_{lsr} (km s^{-1})

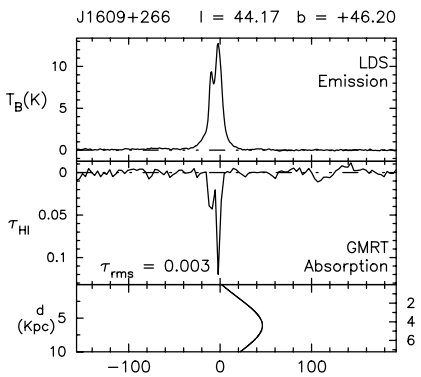
J1609+266 l = 44.17 b = +46.20
LDS
Emission
T_B(K)
GMRT
Absorption
τ_{rms} = 0.003
τ_{HI}
d
(Kpc)

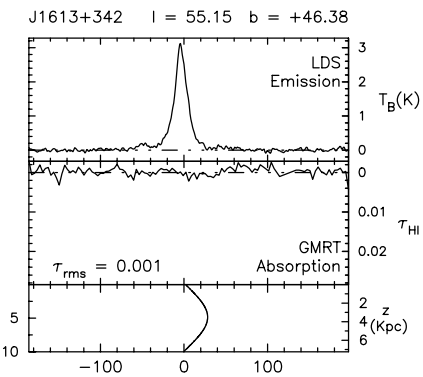
J1613+342 l = 55.15 b = +46.38
LDS
Emission
T_B(K)
GMRT
Absorption
τ_{rms} = 0.001
τ_{HI}
z
(Kpc)

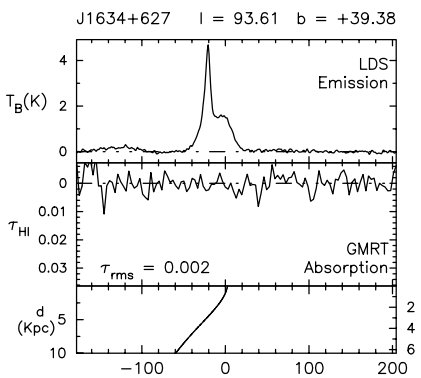
J1634+627 l = 93.61 b = +39.38
LDS
Emission
T_B(K)
GMRT
Absorption
τ_{rms} = 0.002
τ_{HI}
d
(Kpc)

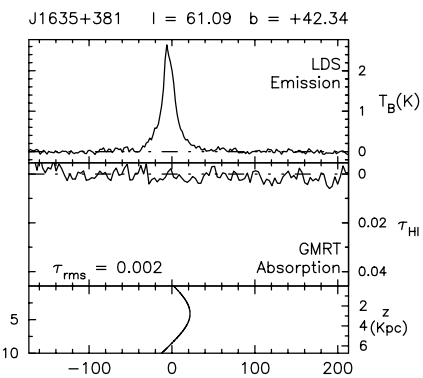
J1635+381 l = 61.09 b = +42.34
LDS
Emission
T_B(K)
GMRT
Absorption
τ_{rms} = 0.002
τ_{HI}
z
(Kpc)

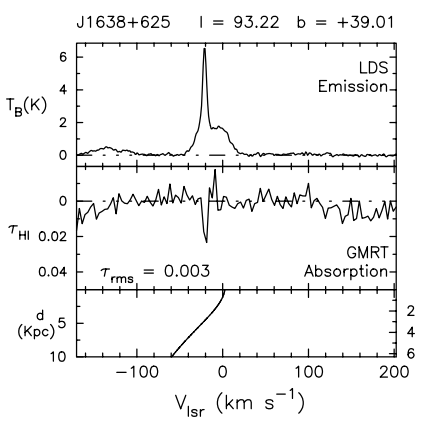
J1638+625 l = 93.22 b = +39.01
LDS
Emission
T_B(K)
GMRT
Absorption
τ_{rms} = 0.003
τ_{HI}
d
(Kpc)
V_{lsr} (km s^{-1})

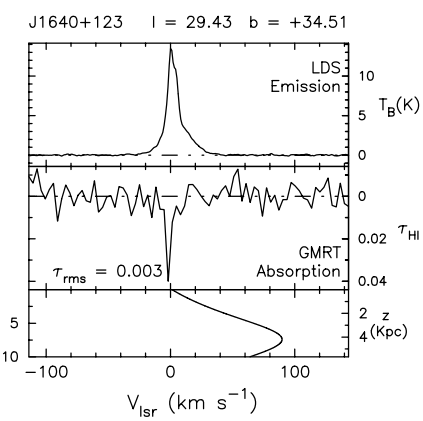
J1640+123 l = 29.43 b = +34.51
LDS
Emission
T_B(K)
GMRT
Absorption
τ_{rms} = 0.003
τ_{HI}
z
(Kpc)
V_{lsr} (km s^{-1})

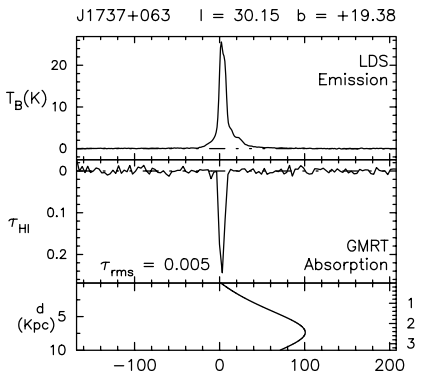
J1737+063 l = 30.15 b = +19.38
LDS
Emission
T_B(K)
τ_{HI}
GMRT
Absorption
τ_{rms} = 0.005
d (Kpc)
z (Kpc)

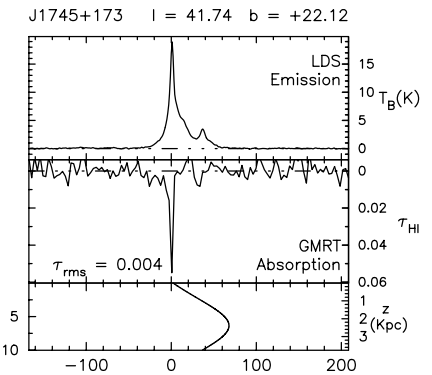
J1745+173 l = 41.74 b = +22.12
LDS
Emission
T_B(K)
τ_{HI}
GMRT
Absorption
τ_{rms} = 0.004
z (Kpc)

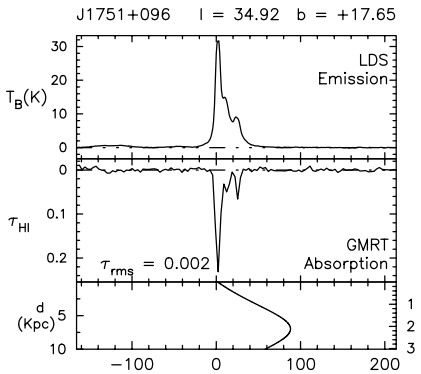
J1751+096 l = 34.92 b = +17.65
LDS
Emission
T_B(K)
τ_{HI}
GMRT
Absorption
τ_{rms} = 0.002
d (Kpc)
z (Kpc)

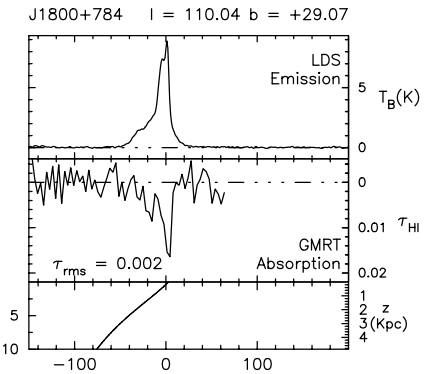
J1800+784 l = 110.04 b = +29.07
LDS
Emission
T_B(K)
τ_{HI}
GMRT
Absorption
τ_{rms} = 0.002
z (Kpc)

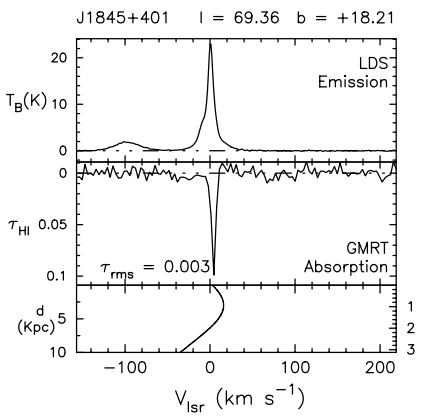
J1845+401 l = 69.36 b = +18.21
LDS
Emission
T_B(K)
τ_{HI}
GMRT
Absorption
τ_{rms} = 0.003
d (Kpc)
V_{lsr} (km s^{-1})

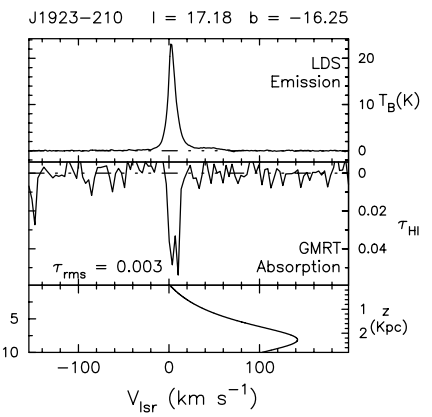
J1923−210 l = 17.18 b = −16.25
LDS
Emission
T_B(K)
τ_{HI}
GMRT
Absorption
τ_{rms} = 0.003
z (Kpc)
V_{lsr} (km s^{-1})

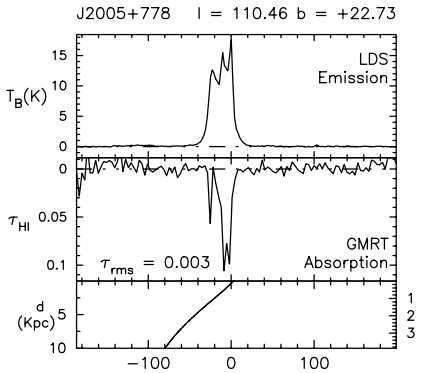
J2005+778 l = 110.46 b = +22.73
LDS
Emission
T_B(K)
GMRT
Absorption
τ_{rms} = 0.003
τ_{HI}
d
(Kpc)

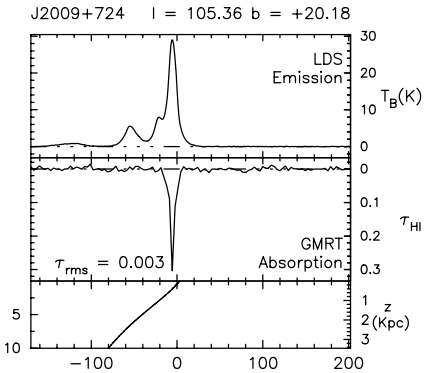
J2009+724 l = 105.36 b = +20.18
LDS
Emission
T_B(K)
GMRT
Absorption
τ_{rms} = 0.003
τ_{HI}
z
(Kpc)

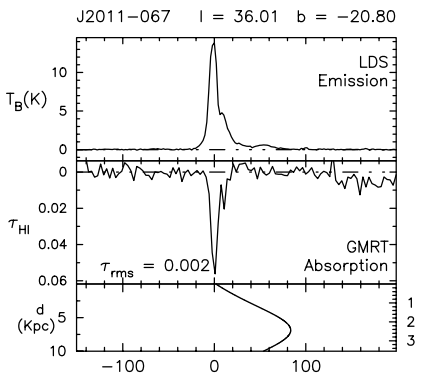
J2011−067 l = 36.01 b = −20.80
LDS
Emission
T_B(K)
GMRT
Absorption
τ_{rms} = 0.002
τ_{HI}
d
(Kpc)

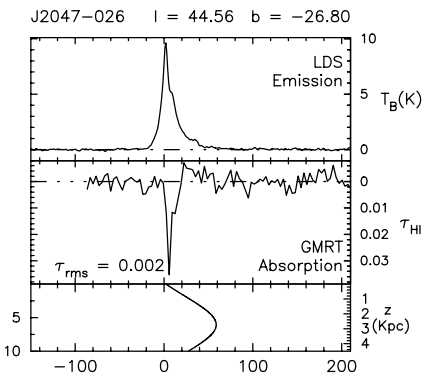
J2047−026 l = 44.56 b = −26.80
LDS
Emission
T_B(K)
GMRT
Absorption
τ_{rms} = 0.002
τ_{HI}
z
(Kpc)

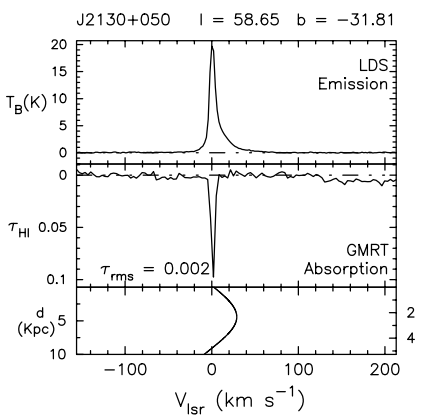
J2130+050 l = 58.65 b = −31.81
LDS
Emission
T_B(K)
GMRT
Absorption
τ_{rms} = 0.002
τ_{HI}
d
(Kpc)
V_{lsr} (km s^{-1})

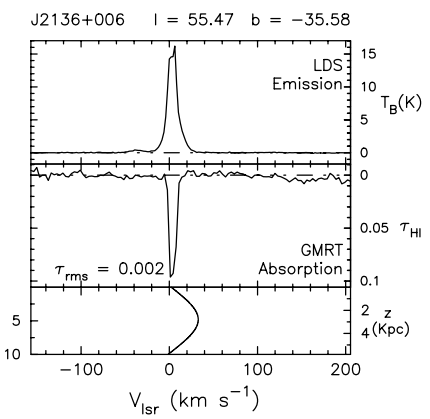
J2136+006 l = 55.47 b = −35.58
LDS
Emission
T_B(K)
GMRT
Absorption
τ_{rms} = 0.002
τ_{HI}
z
(Kpc)
V_{lsr} (km s^{-1})

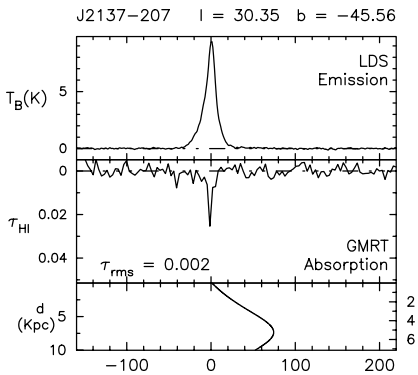
J2137−207 l = 30.35 b = −45.56
LDS
Emission
T_B(K)
τ_{HI}
GMRT
Absorption
τ_{rms} = 0.002
d
(Kpc)

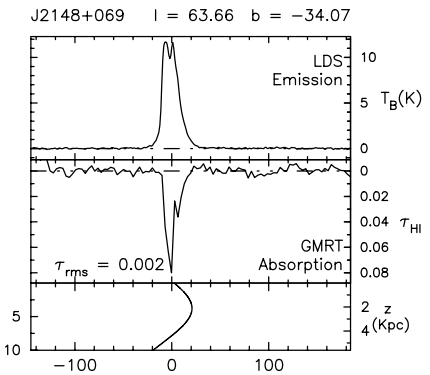
J2148+069 l = 63.66 b = −34.07
LDS
Emission
T_B(K)
τ_{HI}
GMRT
Absorption
τ_{rms} = 0.002
z
(Kpc)

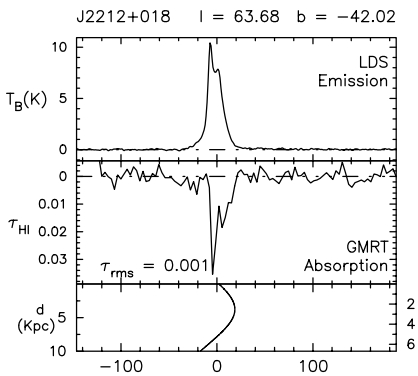
J2212+018 l = 63.68 b = −42.02
LDS
Emission
T_B(K)
τ_{HI}
GMRT
Absorption
τ_{rms} = 0.001
d
(Kpc)

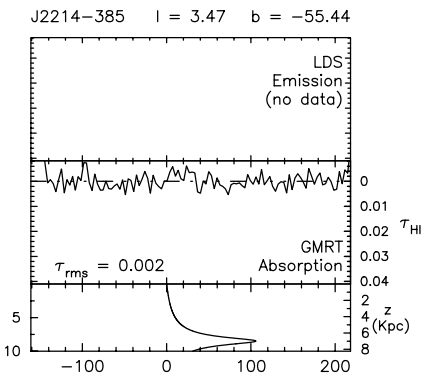
J2214−385 l = 3.47 b = −55.44
LDS
Emission
(no data)
τ_{HI}
GMRT
Absorption
τ_{rms} = 0.002
z
(Kpc)

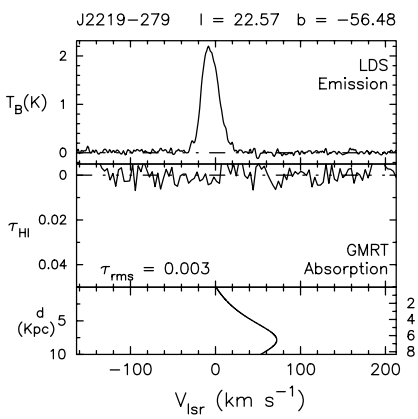
J2219−279 l = 22.57 b = −56.48
LDS
Emission
T_B(K)
τ_{HI}
GMRT
Absorption
τ_{rms} = 0.003
d
(Kpc)
V_{lsr} (km s^{-1})

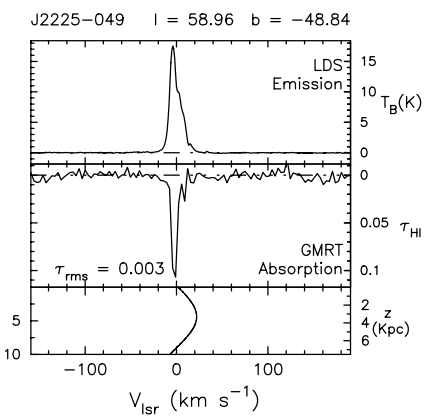
J2225−049 l = 58.96 b = −48.84
LDS
Emission
T_B(K)
τ_{HI}
GMRT
Absorption
τ_{rms} = 0.003
z
(Kpc)
V_{lsr} (km s^{-1})

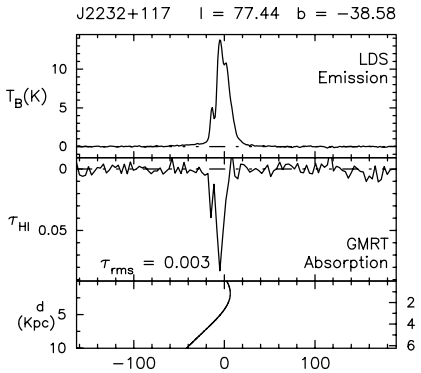
J2232+117 l = 77.44 b = −38.58
LDS
Emission
T_B(K)
τ_{HI}
GMRT
Absorption
τ_{rms} = 0.003
d
(Kpc)
z
(Kpc)

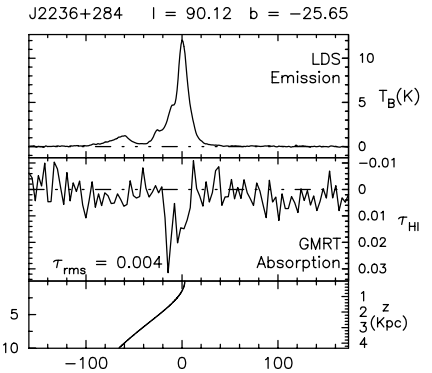
J2236+284 l = 90.12 b = −25.65
LDS
Emission
T_B(K)
τ_{HI}
GMRT
Absorption
τ_{rms} = 0.004
z
(Kpc)

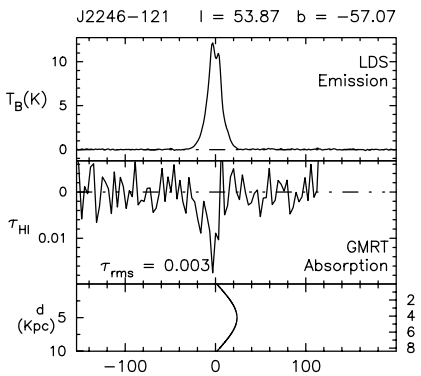
J2246−121 l = 53.87 b = −57.07
LDS
Emission
T_B(K)
τ_{HI}
GMRT
Absorption
τ_{rms} = 0.003
d
(Kpc)
z
(Kpc)

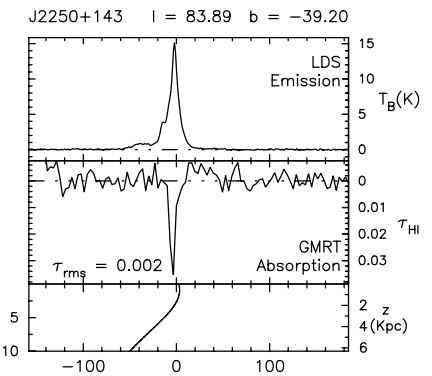
J2250+143 l = 83.89 b = −39.20
LDS
Emission
T_B(K)
τ_{HI}
GMRT
Absorption
τ_{rms} = 0.002
z
(Kpc)

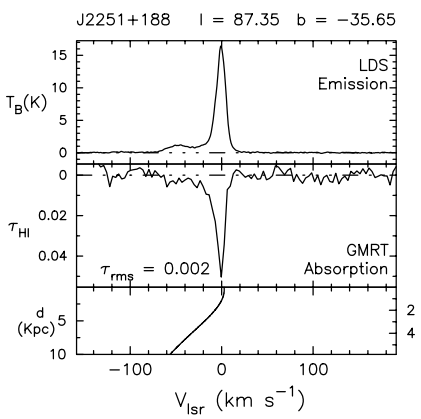
J2251+188 l = 87.35 b = −35.65
LDS
Emission
T_B(K)
τ_{HI}
GMRT
Absorption
τ_{rms} = 0.002
d
(Kpc)
V_{lsr} (km s^{-1})

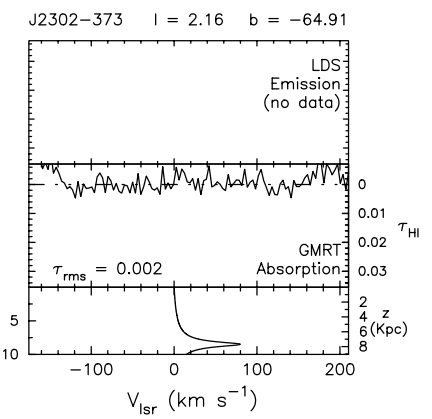
J2302−373 l = 2.16 b = −64.91
LDS
Emission
(no data)
τ_{HI}
GMRT
Absorption
τ_{rms} = 0.002
z
(Kpc)
V_{lsr} (km s^{-1})

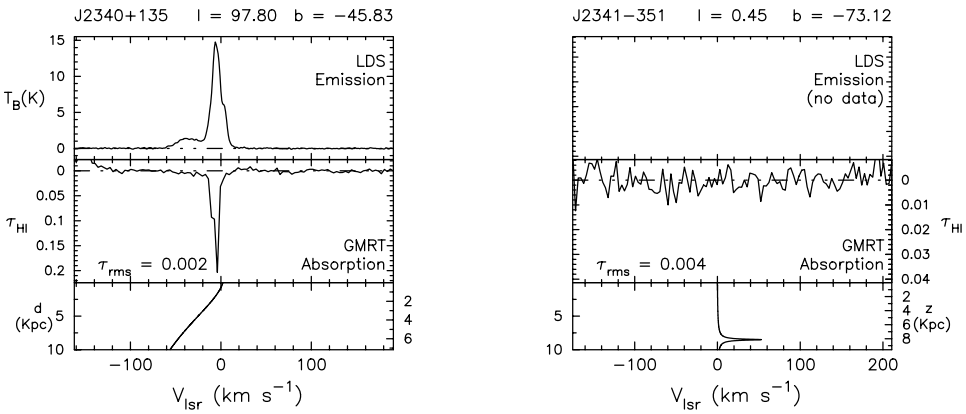

Appendix C

In this Appendix, we list the discrete HI features identified from the high latitude Galactic HI absorption survey using the GMRT and from the HI emission data along the respective lines of sight from the Leiden–Dwingeloo survey of Galactic neutral hydrogen. We have used the HI emission and absorption data to estimate the spin temperature of the absorbing gas.

In the following table, the first column lists the name of the background source, towards which the absorption was measured using the GMRT. Columns 2, 3 and 4 list the peak optical depth, the mean LSR velocity and the FWHM respectively of discrete components identified using Gaussian fitting. The value of FWHM is deconvolved for a channel width of 3.26 km s^{-1}. The unresolved lines are marked with a "–". Columns 5, 6 and 7 list the same for the HI emission profile along the same line of sight, obtained from the Leiden–Dwingeloo survey of Galactic neutral hydrogen (Hartmann & Burton, 1995). The formal 1σ errors estimated in the last digit of the fitted parameters are given within brackets. Column 8 lists the spin temperature, calculated using the absorption and emission data. Column 2 also lists the 3σ optical depth limit obtained from the HI absorption profiles along the respective directions.

	HI Absorption (GMRT)			**HI Emission** (LDS)			
Source	τ_{HI}	V_{lsr} (km s^{-1})	FWHM (km s^{-1})	T_B (K)	V_{lsr} (km s^{-1})	FWHM (km s^{-1})	T_S (K)
J0010 − 418	< 0.006				No data		
J0022 + 002	< 0.009			2.5(2)	−1.1(2)	6.2(4)	> 278
				3.8(2)	−2.2(2)	17.4(4)	> 422
				3.4(9)	−5.89(6)	3.8(3)	> 340
				2.3(6)	−8(1)	7(1)	> 256
				0.40(3)	−17(1)	47(2)	> 44
J0024 − 420	< 0.009				No data		
J0025 − 260	< 0.009			2.8(1)	−5.21(8)	13.3(3)	> 311
				1.1(1)	−8.7(5)	28(1)	> 122
				0.31(1)	−74(1)	55(3)	> 34

Source	**HI Absorption** (GMRT)			**HI Emission** (LDS)			
	$\tau_{\rm HI}$	$V_{\rm lsr}$ (km s^{-1})	FWHM (km s^{-1})	T_B (K)	$V_{\rm lsr}$ (km s^{-1})	FWHM (km s^{-1})	T_S (K)
J0029 + 349	< 0.006			8.27(7)	+2.7(1)	10.9(2)	> 1378
	0.193(5)	−2.02(6)	3.3(2)	16.1(2)	−3.68(1)	5.11(5)	29
				2.58(7)	−12.68(5)	4.5(1)	> 430
				1.23(3)	−20.2(8)	55(1)	> 205
				1.35(4)	−39.8(2)	14.1(6)	> 225
J0059 + 001	0.09(1)	−7.6(4)	–	3.59(9)	−7.50(3)	5.1(1)	42
	< 0.012			5.14(8)	−7.60(4)	14.9(2)	> 428
				0.78(2)	−21.4(8)	51(1)	> 65
				0.24(3)	−46.2(5)	9(1)	> 20
J0116 − 208	< 0.009			2.48(5)	−6.57(8)	15.1(3)	> 276
	0.030	−5.79	–	2.32(5)	−7.15(3)	3.7(1)	78
				0.44(4)	−14(1)	38(2)	> 49
				0.118(9)	−69(7)	127(11)	> 13
J0119 + 321	0.08(4)	+2.8(8)	–	8.0(2)	+2.81(1)	3.62(5)	104
	< 0.009			5.9(5)	−0.4(4)	12.5(3)	> 656
	0.034(7)	−3(3)	7(5)	7.9(5)	−3.41(4)	6.0(1)	236
				5.7(1)	−14.6(2)	15.3(4)	> 633
				0.93(7)	−29.9(7)	66(2)	> 103
				0.40(4)	−46.6(6)	17(2)	> 44
				0.17(2)	−86.6(7)	11(2)	> 19
J0137 + 331	< 0.009			2.99(9)	+2.46(3)	3.9(1)	> 322
	0.037(5)	−2.6(5)	6(1)	0.6(2)	−3.3(2)	4.6(9)	17
				8.2(2)	−3.7(1)	17.5(2)	> 910
	0.020(4)	−13(1)	7(3)	1.7(2)	−13.1(2)	6.9(5)	86
				0.82(4)	−15.0(7)	49(1)	> 91
J0204 + 152	< 0.009			4.8(1)	−0.37(6)	6.0(1)	> 533
				4.0(3)	−5.0(1)	18.4(3)	> 444
	0.057(4)	−6.8(3)	9(7)	14.0(3)	−7.61(5)	8.4(2)	253
				1.7(2)	−12.21(6)	4.0(3)	> 189
				0.31(1)	−48.7(4)	23(1)	> 34
				0.104(9)	−111(2)	45(4)	> 12
J0204 − 170	0.054(6)	0.0(3)	5(1)	8.90(4)	+2.05(1)	4.43(3)	169
	< 0.009			3.81(5)	−4.47(8)	18.4(1)	> 423
				1.91(5)	−9.73(6)	6.5(2)	> 212
				0.136(9)	−20(2)	117(6)	> 15
J0237 + 288	< 0.009			7(1)	+4.5(9)	8.7(8)	> 778
				14(2)	+3.25(7)	3.8(1)	> 280
	0.347(7)	−2.12(5)	4.7(2)	21(2)	−0.01(9)	4.9(2)	72

Source	**HI Absorption** (GMRT)			**HI Emission** (LDS)			
	$\tau_{\rm HI}$	$V_{\rm lsr}$ (km s^{-1})	FWHM (km s^{-1})	T_B (K)	$V_{\rm lsr}$ (km s^{-1})	FWHM (km s^{-1})	T_S (K)
				2.56(7)	−3.9(2)	27.8(4)	> 284
	0.127(7)	−10.0(2)	3.5(3)	12.6(2)	−5.78(5)	5.28(7)	106
				0.16(1)	−10(3)	140(9)	> 18
J0238 + 166	< 0.012			17.1(1)	−0.38(2)	15.46(6)	> 1425
	0.122(8)	−2.8(1)	4.7(4)	10.6(1)	−1.49(1)	5.52(5)	92
				0.14(1)	−22(5)	115(10)	> 12
J0240 − 231	0.04(1)	+1.4(5)	4(1)	1.83(6)	−1.13(4)	5.01(1)	47
	< 0.009			2.1(1)	−5.2(2)	21.4(4)	> 233
				4.9(1)	−10.51(3)	9.5(1)	> 544
				0.152(7)	−33(2)	124(5)	> 17
J0318 + 164	0.095(8)	+7.5(2)	4.0(7)	2.7(1)	+7.86(6)	3.7(2)	30
	< 0.006			23.9(3)	+1.49(2)	13.06(8)	> 3983
	0.404(5)	+0.23(4)	4.6(1)	14.9(3)	−0.17(2)	5.63(6)	45
				1.5(1)	−1.1(4)	31(1)	> 250
				0.11(1)	−57(8)	85(17)	> 18
J0321 + 123	1.5(1)	+8.1(1)	6.2(1)	47(2)	+10.74(4)	6.71(7)	60
	0.39(5)	+2(1)	9(1)	44.4(6)	+4.5(1)	10.5(2)	137
	< 0.006			1.6(3)	+2.2(7)	30(3)	> 267
				3.6(2)	−6.5(1)	4.4(3)	> 600
				0.17(3)	−111(7)	80(16)	> 28
J0323 + 055	0.21(2)	+9.2(2)	–	23.8(4)	+12.51(1)	4.22(4)	126
	< 0.009			10(2)	+6.4(6)	14.4(8)	> 1111
	0.229(9)	+3.3(2)	5.5(4)	12.7(5)	+6.29(3)	4.33(8)	62
				17.9(7)	−4.65(8)	7.8(1)	> 1989
				2(1)	−5(9)	21(7)	> 222
	0.500(5)	−8.64(3)	4.62(6)	6.6(4)	−7.35(3)	3.9(1)	17
				0.176(8)	−57(4)	117(7)	> 20
J0329 + 279	0.25(2)	+3.3(2)	–	22.1(3)	+6.96(1)	4.12(4)	100
	< 0.009			25.7(5)	+4.57(3)	12.91(9)	> 2855
	0.23(2)	−2.8(3)	3.7(8)	15.7(4)	+1.18(3)	6.04(8)	76
				1.24(2)	−14.9(6)	56(1)	> 138
J0336 + 323	2.62(1)	+6.698(8)	3.7(3)	33.7(4)	+8.36(4)	5.57(4)	36
	< 0.012			9.8(2)	+5.30(6)	15.3(2)	> 817
				33.2(5)	+4.42(3)	4.96(3)	> 36
				2.6(2)	−20.4(6)	48.2(8)	> 217
J0348 + 338	< 0.009			15.3(5)	+10.30(2)	3.29(5)	> 1700
	1.33(2)	+7.69(2)	–	38.76(7)	+7.52(6)	6.22(7)	53
	0.07(2)	+7.1(5)	13(2)	3.5(2)	+7.5(1)	15.1(6)	52

Source	**HI Absorption** (GMRT)			**HI Emission** (LDS)			
	$\tau_{\rm HI}$	$V_{\rm lsr}$ (km s^{-1})	FWHM (km s^{-1})	T_B (K)	$V_{\rm lsr}$ (km s^{-1})	FWHM (km s^{-1})	T_S (K)
				7.1(9)	+5.57(3)	2.7(1)	> 789
				1.2(3)	+1.5(2)	2.6(3)	> 133
				2.73(6)	−18.81(3)	5.5(1)	> 303
				3.0(1)	−19.1(6)	44.0(5)	> 333
				2.2(1)	−19.8(2)	17.0(7)	> 244
J0403 + 260	0.305(5)	+7.61(6)	3.78(1)	13.8(1)	+7.61(7)	3.47(3)	52
	< 0.012			6.1(2)	+4.85(7)	21.6(3)	> 508
				9.8(2)	+3.94(6)	9.3(1)	> 817
				0.31(5)	−20(2)	99(7)	> 26
				1.42(5)	−29.9(5)	25(2)	> 118
				1.19(9)	−45.9(2)	11.3(6)	> 99
J0409 + 122	< 0.009			11.0(2)	+11.41(6)	3.4(1)	> 1222
				28(1)	+8.9(1)	4.9(2)	> 3111
	1.25(1)	+5.9(1)	3.5(2)	30.9(8)	+6.40(3)	9.68(4)	43
	0.22(2)	0.0(6)	5.6(7)	8.7(3)	+1.43(4)	3.97(7)	44
				0.14(2)	−21(4)	75(6)	> 16
J0410 + 769	< 0.006			0.5(2)	+18(1)	13.2(4)	> 56
				3.9(3)	+3.62(7)	3.3(1)	> 650
	0.230(3)	−0.88(5)	3.78(8)	17.4(8)	−0.40(2)	5.4(1)	85
				9.8(8)	−2.3(3)	11.6(7)	> 1633
				8.2(4)	−7.0(6)	24.9(5)	> 1366
	0.069(3)	−11.5(2)	6.9(5)	6.6(2)	−11.85(4)	4.9(1)	99
				0.52(2)	−57.4(6)	34(2)	> 58
				1.14(2)	−99.4(4)	23.5(9)	> 127
				1.20(2)	−127.5(4)	24.7(8)	> 133
J0424 + 020	< 0.012			8.9(5)	+11.92(5)	3.8(1)	> 741
	0.523(5)	+5.63(3)	5.4(7)	12.4(8)	+7.96(9)	12.5(3)	30
				5.8(7)	+6.93(3)	3.1(2)	> 483
				4.4(2)	+3.7(2)	24.4(3)	> 367
	0.5(3)	+2.2(9)	–	10.9(4)	+2.36(4)	4.36(7)	28
				0.37(1)	−46.3(6)	30(2)	> 31
J0431 + 406	< 0.009			8.4(7)	+11.92(2)	2.84(9)	> 933
	1.19(3)	+10.01(2)	–	27.1(6)	+9.47(5)	5.32(9)	39
				29(1)	+4.27(4)	14.5(2)	> 3222
	0.70(1)	+3.61(4)	4.4(1)	34(1)	+4.09(4)	8.2(1)	68
				3.7(1)	−6.3(8)	41(1)	> 411
				0.5(1)	−31.9(5)	16(2)	> 56
				0.14(1)	−98(4)	74(9)	> 16

Source	**HI Absorption** (GMRT)			**HI Emission** (LDS)			
	τ_{HI}	V_{lsr} (km s^{-1})	FWHM (km s^{-1})	T_B (K)	V_{lsr} (km s^{-1})	FWHM (km s^{-1})	T_S (K)
J0440 − 435	< 0.009			No data			
J0453 − 281	< 0.012			3.3(1)	+1.19(7)	19.0(3)	> 275
				5.1(1)	+1.14(3)	7.1(1)	> 425
				0.11(1)	−25(5)	136(11)	> 9
J0459 + 024	0.080(5)	+11.1(2)	–	19.2(1)	+10.44(1)	5.40(4)	250
	< 0.009			7.1(4)	+6.7(1)	22.7(6)	> 789
				1.9(2)	−12(3)	40(3)	> 211
	0.026(4)	−25.6(5)	–	0.21(8)	−28(1)	6(3)	8
J0503 + 020	< 0.009			6.1(2)	+10.53(7)	6.0(1)	> 508
				10.0(1)	+10.25(5)	18.0(1)	> 833
	0.26(9)	+9.92(6)	–	12.0(2)	+9.03(1)	2.98(4)	52
				2.40(3)	−12.8(4)	31.6(8)	> 200
				0.08(2)	−31(8)	131(18)	> 7
J0538 − 440	< 0.006			No data			
J0541 − 056	< 0.012			37.8(1)	+4.19(4)	5.97(3)	> 3150
	0.842(5)	+7.44(2)	6.06(5)	16(2)	+7.5(1)	6.1(2)	28
				12.6(2)	+8.23(3)	23.3(2)	> 1050
				23(2)	+8.9(2)	9.6(2)	> 1917
				0.48(4)	+9.9(8)	74(3)	> 40
	0.069(7)	+17.8(9)	–				
J0609 − 157	< 0.021			6.7(2)	+3.10(2)	2.97(6)	> 319
				18.6(3)	+7.057(9)	3.71(4)	> 885
	0.432(9)	+10.51(8)	7.1(2)	20.3(4)	+8.37(5)	10.2(1)	58
				6.6(2)	+12.2(1)	26.6(6)	> 314
				4.8(1)	+18.89(5)	5.9(1)	> 229
				1.7(1)	+25.5(9)	52.5(8)	> 81
J0614 + 607	0.09(2)	+10.1(8)	–	7.96(5)	+9.40(1)	4.69(4)	88
	< 0.015			1.4(1)	+1.34(6)	2.5(2)	> 93
	0.29(1)	+02.2(2)	10.7(6)	25.9(1)	+0.410(8)	7.72(2)	103
				5.17(4)	−7.1(1)	29.3(2)	> 345
				0.68(5)	−18.6(2)	7.9(6)	> 45
				1.30(2)	−49.1(2)	20.8(6)	> 87
				1.21(2)	−79.9(3)	30.0(7)	> 81
J0713 + 438	< 0.012			3.1(2)	+14.57(3)	4.1(1)	> 258
				6.3(1)	+12.9(2)	11.0(3)	> 525
	0.015(3)	+5(3)	27(6)	6.5(3)	−1.57(2)	4.03(9)	433
				3.6(4)	−4.7(2)	9.3(3)	> 300
				7.5(2)	−6.6(4)	29.0(4)	> 625

Source	**HI Absorption** (GMRT)			**HI Emission** (LDS)			
	$\tau_{\rm HI}$	$V_{\rm lsr}$ (km s^{-1})	FWHM (km s^{-1})	T_B (K)	$V_{\rm lsr}$ (km s^{-1})	FWHM (km s^{-1})	T_S (K)
				3.9(1)	−12.27(4)	5.5(1)	> 325
				0.66(5)	−36(1)	22(1)	> 55
J0814 + 459	0.035(2)	+16.8(9)	–	9.5(5)	+15.4(1)	3.8(1)	276
	< 0.015			3.4(2)	+12.8(3)	12.6(7)	> 226
				4.0(6)	+12.6(2)	3.5(2)	> 267
				1.1(2)	+2.9(1)	5.0(5)	> 73
				5.38(7)	−2.9(2)	13.5(3)	> 359
				0.64(3)	−12(1)	55(2)	> 43
J0825 + 031	< 0.006			0.24(2)	+27(3)	84(5)	> 40
				1.6(2)	+19(1)	15(1)	> 267
	0.034(7)	+14.8(6)	4(1)	8.6(2)	+16.70(2)	4.93(8)	257
	0.043(7)	+4.9(7)	–	6.4(6)	+5.3(1)	9.7(5)	152
				3.1(3)	−3(1)	13(1)	> 207
J0834 + 555	< 0.006			0.111(8)	+61(10)	123(20)	> 19
				0.7(2)	+13(3)	15(3)	> 117
	0.059(3)	+1.4(2)	3.4(3)	12.7(1)	+3.005(9)	4.89(4)	222
				5.4(2)	−1.0(4)	14.8(5)	> 900
	0.016(4)	−39(1)	–	0.97(6)	−40(2)	30(4)	61
				1.74(7)	−55.44(8)	5.9(2)	> 290
				1.6(2)	−58.7(5)	17.9(9)	> 267
J0842 + 185	< 0.012			0.21(2)	+29(2)	21(4)	> 18
				3.54(2)	+0.3(1)	25.5(3)	> 295
				0.84(5)	−14.5(1)	4.4(3)	> 70
J0854 + 201	< 0.006			0.7(2)	+11(2)	11(2)	> 117
				1.2(1)	+6.15(8)	4.8(3)	> 200
				4.7(1)	+0.4(3)	14.1(3)	> 783
				0.70(2)	−12.6(8)	49(1)	> 117
				0.30(2)	−32.9(3)	10.0(9)	> 50
J0921 − 263	0.15(1)	−1.7(8)	–	19.1(4)	−1.77(8)	10.1(2)	137
	< 0.009			9.4(5)	−3.00(2)	4.3(1)	> 1044
	0.022(6)	+5(4)	5(9)	6.1(2)	+6.78(9)	6.4(1)	280
				3.4(2)	+11.0(5)	31(1)	> 378
				1.3(1)	+23(2)	55(1)	> 144
J0958 + 324	< 0.015			1.27(1)	+0.2(1)	28.0(4)	> 85
				0.83(1)	−41.9(2)	25.6(6)	> 55
				1.16(1)	−86.4(1)	24.9(3)	> 77
J1018 − 317	< 0.006			0.66(6)	+24(3)	80(3)	> 73
	0.109(6)	+13.5(1)	–	5.0(3)	+6.3(2)	20.6(6)	48

Source	**HI Absorption** (GMRT)			**HI Emission** (LDS)			
	$\tau_{\rm HI}$	$V_{\rm lsr}$ (km s^{-1})	FWHM (km s^{-1})	T_B (K)	$V_{\rm lsr}$ (km s^{-1})	FWHM (km s^{-1})	T_S (K)
				2.3(3)	−1(1)	36(2)	> 256
	0.035(3)	−7.0(3)	5.7(8)	8.4(1)	−7.36(4)	9.5(1)	240
J1057 − 245	0.063(7)	−3.0(4)	–	14.2(2)	−4.118(8)	3.82(3)	233
	< 0.012			7.7(2)	−5.65(9)	10.2(2)	> 642
				1.3(1)	−14.6(4)	41(2)	> 108
				3.7(3)	−20.84(7)	6.9(3)	> 308
				5.9(3)	−21.2(1)	14.4(4)	> 492
J1111 + 199	< 0.009			0.23(1)	+12(3)	96(4)	> 26
				0.70(2)	−2.1(4)	6.4(8)	> 78
				1.2(2)	−3.21(8)	3.3(2)	> 133
				1.35(6)	−7.2(6)	19(1)	> 150
				0.4(1)	−23(1)	10(3)	> 44
				1.2(8)	−34.2(4)	12(3)	> 133
				0.7(5)	−41(8)	19(6)	> 78
J1119 − 030	0.034(3)	−8.2(3)	3.7(4)	3.1(3)	−3(1)	14(1)	93
	< 0.006			6.4(6)	+5.3(1)	9.7(5)	> 1067
				8.6(2)	+16.70(2)	4.93(8)	> 1433
				1.6(2)	+19(1)	15(1)	> 267
				0.24(2)	+27(3)	84(5)	> 40
J1120 − 251	< 0.009			0.11(1)	+16(5)	105(10)	> 12
	0.020(4)	−2(1)	–	5(1)	−2.74(3)	4.2(2)	253
				4.9(9)	−2.77(4)	6.9(4)	> 544
				4.95(4)	−9.3(1)	23.4(2)	> 550
				1.85(6)	−21.47(7)	7.3(2)	> 206
J1125 + 261	< 0.009			0.088(6)	+51(3)	74(8)	> 10
				1.36(1)	−7.2(1)	22.5(3)	> 151
				0.857(9)	−45.6(2)	30.9(5)	> 95
J1130 − 148	< 0.006			0.21(2)	−9(2)	103(6)	> 35
	0.007(1)	+7(3)	37(6)	3.9(1)	−7.13(4)	8.9(2)	557
				4.7(1)	−6.72(8)	20.3(4)	> 783
				1.22(2)	+20.1(2)	19.8(5)	> 203
J1146 + 399	< 0.027			0.110(7)	+55(3)	75(8)	> 4
				0.82(2)	−7.2(3)	25.4(8)	> 30
				1.11(1)	−43.0(4)	33.7(7)	> 41
				1.77(3)	−55.11(5)	7.7(1)	> 66
J1154 − 350	0.022(3)	+3.7(4)	8(1)				
	0.092(4)	−8.3(1)	4.2(4)		No data		
	0.016(3)	−16(2)	13(5)				

Source	**HI Absorption** (GMRT)			**HI Emission** (LDS)			
	$\tau_{\rm HI}$	$V_{\rm lsr}$ (km s^{-1})	FWHM (km s^{-1})	T_B (K)	$V_{\rm lsr}$ (km s^{-1})	FWHM (km s^{-1})	T_S (K)
J1221 + 282	< 0.012			0.77(3)	−1.4(2)	9.0(5)	> 64
	0.01(0)	−20(0)	–	0.47(4)	−18.9(4)	11(1)	47
				1.52(3)	−26.3(7)	43.2(7)	> 127
	0.02(0)	−38(0)	–	1.06(4)	−34.8(1)	6.1(3)	53
				0.89(4)	−46.9(3)	16.0(9)	> 74
J1235 − 418	0.132(7)	−14.2(2)	8.1(5)		No data		
J1254 + 116	< 0.015			3.1(3)	+2.4(4)	8.7(3)	> 207
	0.03(1)	−5.9(8)	4(2)	6.3(6)	−3.49(3)	5.1(1)	213
				2.3(5)	−6(1)	10(1)	> 153
				0.92(2)	−14.7(5)	41.3(8)	> 61
				0.082(9)	−80(3)	48(8)	> 5
J1257 − 319	0.108(6)	−16.0(2)	–		No data		
J1316 − 336	0.042(9)	−8.5(7)	4(1)		No data		
J1344 + 141	< 0.009			1.40(5)	+00.40(5)	3.9(1)	> 156
				3.20(6)	−03.9(1)	12.7(2)	> 356
				0.14(3)	−08(2)	93(9)	> 11
				1.1(1)	−10.7(4)	30(1)	> 122
J1351 − 148	0.19(3)	−05.5(1)	3.4(1)	17.2(5)	−04.52(2)	4.4(1)	90
	< 0.009			10.9(5)	−04.4(1)	11.0(3)	> 1211
				3.1(1)	−02.8(5)	41(1)	> 344
	0.020(4)	+22.0(6)	4(1)	5.7(1)	+22.9(1)	10.5(2)	285
J1357 − 154	0.40(2)	−2.1(2)	–	25.1(1)	−3.779(7)	5.75(3)	76
	< 0.045			6.6(5)	−2.6(2)	18.5(7)	> 147
				5(2)	+20.2(3)	10.0(9)	> 111
				1.2(3)	−18(5)	30(5)	> 27
				0.9(1)	+26(12)	15(9)	> 20
J1435 + 760	< 0.009			0.08(1)	+9(10)	146(15)	> 9
				1.51(3)	+0.42(8)	11.0(2)	> 168
				1.82(2)	−12.3(3)	39.0(6)	> 202
				0.60(4)	−38.5(5)	11(1)	> 67
				0.26(3)	−51(1)	12(3)	> 29
				1.94(2)	−69.8(1)	18.6(3)	> 216
				0.08(1)	−137(2)	16(4)	> 9
J1445 + 099	< 0.006			2.68(5)	+0.36(9)	17.3(3)	> 447
				3.44(4)	−2.81(2)	5.14(7)	> 573
				0.35(4)	−8(1)	46(3)	> 58
J1448 − 163	< 0.009			0.29(3)	+10(2)	77(4)	> 32
				3.1(2)	+6.03(4)	4.7(2)	> 344

Source	**HI Absorption** (GMRT)			**HI Emission** (LDS)			
	$\tau_{\rm HI}$	$V_{\rm lsr}$ (km s^{-1})	FWHM (km s^{-1})	T_B (K)	$V_{\rm lsr}$ (km s^{-1})	FWHM (km s^{-1})	T_S (K)
				11.3(5)	−1.63(5)	19.8(3)	> 1256
	0.203(8)	−4.60(7)	–	12.1(4)	−3.37(4)	7.9(2)	66
	0.05(3)	−12(2)	–	8.9(1)	−6.00(1)	3.08(4)	182
				1.91(4)	−22.6(1)	6.7(2)	> 212
J1506 + 375	< 0.009			0.28(2)	−53(1)	33(3)	> 33
				0.98(3)	−07.1(5)	31(1)	> 111
				1.64(4)	+00.2(1)	8.9(3)	> 177
				0.13(1)	+57(2)	44(6)	> 11
J1513 + 236	0.15(3)	00.0(1)	–	9.5(1)	−00.9(1)	9.2(1)	63
	< 0.006			1.1(1)	−03.4(4)	23(1)	> 183
	0.26(5)	−05.73(5)	–	15.8(1)	−04.06(1)	3.23(2)	61
				0.22(2)	−19(4)	84(8)	> 33
J1517 − 243	< 0.012			13.2(6)	+2.3(2)	5.2(2)	> 667
				6.2(1)	−1.1(2)	29.0(2)	> 517
	0.071(5)	−1.1(3)	5.7(6)	14(1)	−1.3(1)	4.0(3)	204
	0.105(6)	−7.5(6)	3.8(3)	16(1)	−4.92(8)	3.9(3)	161
				5.8(9)	−8.3(3)	4.0(4)	> 483
				2.1(1)	−14.7(2)	10.0(1)	> 175
J1520 + 202	< 0.009			8.7(6)	−2.7(1)	6.9(2)	> 967
				3.7(4)	−2.78(9)	13.8(5)	> 411
	0.409(7)	−5.28(5)	–	19.4(5)	−5.331(8)	3.83(4)	58
				0.49(2)	−17(1)	52(1)	> 54
J1526 − 138	< 0.006			1.32(4)	+18.6(1)	8.5(4)	> 220
	0.073(9)	+4.4(3)	4.3(9)	15.6(3)	+4.07(1)	4.51(4)	222
				11.7(5)	0.0(1)	15.4(3)	> 1950
	0.092(8)	−1.1(7)	–	13.3(5)	−0.76(2)	4.02(8)	151
				1.90(9)	−3.3(4)	44.5(9)	> 317
				0.8(2)	−5.9(2)	2.3(5)	> 133
	0.029(5)	−7(3)	9(5)	6.4(2)	−9.15(5)	4.8(1)	224
				0.16(1)	−82(2)	45(5)	> 27
J1553 + 129	0.010(1)	+6(4)	26(5)	3.1(1)	+11.0(2)	7.3(4)	312
	0.021(5)	+2.4(7)	5(3)	3.1(3)	+1.0(1)	4.6(4)	148
	< 0.009			6.8(3)	−0.7(2)	7.3(4)	> 756
				0.94(5)	−9(1)	51(2)	> 104
J1554 − 270	< 0.009			3.7(4)	+15.1(7)	9(1)	> 411
	0.259(6)	+1.2(2)	–	28.5(9)	+2.68(4)	4.4(1)	125
				10.8(9)	−4.1(7)	21(1)	> 1200
				11.1(9)	−4.2(1)	6.3(5)	> 1233

Source	**HI Absorption** (GMRT)			**HI Emission** (LDS)			
	$\tau_{\rm HI}$	$V_{\rm lsr}$ (km s^{-1})	FWHM (km s^{-1})	T_B (K)	$V_{\rm lsr}$ (km s^{-1})	FWHM (km s^{-1})	T_S (K)
				0.8(3)	−5(5)	73(17)	> 89
	0.04(2)	−16(8)	8(5)				
J1557 − 000	0.371(8)	+0.34(7)	5.4(1)	28.0(3)	−1.19(4)	6.88(6)	90
	< 0.012			5.1(3)	+0.2(6)	22.6(5)	> 425
				10.5(2)	+1.37(3)	2.6(2)	> 875
				1.3(4)	+13.8(3)	9(1)	> 108
				1.8(3)	+19(2)	19(2)	> 150
J1602 + 334	< 0.006			7.5(2)	−0.03(3)	3.65(4)	> 1250
				3.11(6)	−2.77(7)	16.0(2)	> 518
	0.111(4)	−3.0(1)	5.6(3)	6.14(9)	−3.49(6)	4.51(8)	58
				0.143(7)	−19(2)	149(5)	> 24
				0.66(2)	−21.1(2)	12.7(5)	> 110
J1609 + 266	< 0.009			0.11(2)	+43(1)	13(3)	> 12
	0.123(5)	−1.7(2)	–	9.39(8)	−1.90(1)	7.79(5)	81
				3.36(8)	−5.42(8)	23.8(3)	> 373
	0.056(9)	−10(2)	4(1)	5.86(6)	−9.99(2)	4.26(4)	108
				0.152(6)	−63(5)	133(10)	> 17
J1613 + 342	< 0.003			2.14(6)	−3.48(8)	19.9(4)	> 713
				0.80(6)	−4.5(1)	7.4(5)	> 267
				0.18(2)	−7(2)	83(5)	> 60
				0.10(2)	−49.9(8)	9(2)	> 33
J1634 + 627	< 0.002			1.51(2)	−1.6(4)	22.2(7)	> 252
				2.73(5)	−20.91(4)	6.1(1)	> 455
				1.72(7)	−23.2(4)	19.4(5)	> 287
				0.19(1)	−128(1)	44(3)	> 32
J1635 + 381	< 0.006			0.09(2)	+2(5)	105(15)	> 15
				0.92(8)	−0.3(6)	7.7(9)	> 153
				1.03(5)	−4.7(3)	29(1)	> 172
				1.3(1)	−6.7(3)	6.4(5)	> 217
J1638 + 625	< 0.009			1.64(3)	−1.6(4)	22.6(7)	> 182
	0.028(4)	−20.1(4)	4(1)	4.50(6)	−21.05(2)	5.05(7)	161
				1.97(7)	−23.1(3)	19.0(5)	> 219
				0.40(1)	−133.0(7)	46(2)	> 44
J1640 + 123	0.040(5)	−1.5(4)	–	3.7(5)	+0.13(4)	3.1(2)	94
	< 0.009			6.6(6)	+0.9(2)	8.1(2)	> 733
				3.1(4)	+4.7(1)	3.7(3)	> 344
				3.76(5)	+5.49(9)	26.5(2)	> 418
J1737 + 063	0.258(7)	+2.63(9)	6.0(2)	19.8(1)	+1.62(3)	4.65(4)	87

Source	**HI Absorption** (GMRT)			**HI Emission** (LDS)			
	$\tau_{\rm HI}$	$V_{\rm lsr}$ (km s^{-1})	FWHM (km s^{-1})	T_B (K)	$V_{\rm lsr}$ (km s^{-1})	FWHM (km s^{-1})	T_S (K)
	< 0.015			14.6(1)	+6.02(3)	4.41(5)	> 973
				4.69(6)	+6.8(1)	26.1(3)	> 313
				0.59(5)	+20(2)	64(3)	> 39
J1745 + 173	0.060(8)	0.0(4)	–	11.2(1)	+0.80(1)	4.27(4)	192
	< 0.012			5.7(1)	+3.3(1)	20.2(4)	> 475
				2.2(1)	+14.7(9)	48(1)	> 183
				2.0(2)	+36.9(2)	6.0(4)	> 167
				0.6(1)	+44(2)	12(3)	> 50
J1751 + 096	0.066(3)	+25.6(2)	3.3(2)	3.9(1)	+25.1(1)	7.1(3)	61
	< 0.006			0.32(8)	+25(7)	91(13)	> 53
				7.5(2)	+13.1(2)	29.9(5)	> 1250
	0.051(3)	+12.7(2)	6.2(6)	7.0(2)	+10.54(6)	7.4(3)	141
	0.235(3)	+2.02(5)	5.5(1)	27.6(1)	+1.91(2)	6.43(4)	132
				0.28(5)	−47(2)	22(6)	> 47
				0.56(9)	−112(4)	28(6)	> 93
				0.5(1)	−137(5)	26(6)	> 83
J1800 + 784	0.016(2)	+1.4(7)	9(2)	5.3(1)	+1.58(3)	4.23(6)	334
	< 0.006			4.41(6)	−4.04(7)	7.7(2)	> 735
				3.04(6)	−6.3(3)	27.5(6)	> 507
				0.98(5)	−30.3(5)	18.9(7)	> 163
J1845 + 401	0.099(5)	+4.3(1)	4.6(3)	11.0(3)	+1.3(1)	10.4(1)	117
	< 0.009			2.93(7)	+1.3(1)	36.1(4)	> 326
				9.5(3)	+0.36(2)	4.84(8)	> 320
				3.2(1)	−9.0(2)	9.2(4)	> 356
				1.81(1)	−97.4(1)	36.3(3)	> 201
J1923 − 210	0.053(7)	+2.5(6)	5(2)	10.2(2)	+2.24(5)	4.66(9)	192
	< 0.009			11.7(2)	+3.78(3)	12.7(2)	> 1300
	0.055(8)	+9.7(6)	3.4(7)	1.9(2)	+5.7(1)	3.2(3)	35
				1.8(1)	+7.4(4)	35(1)	> 200
				0.58(2)	+47.4(6)	22(1)	> 64
J2005 + 778	0.07(2)	−3(1)	–	9.3(1)	0.07(2)	3.90(5)	138
	0.05(3)	−7(2)	16(3)	5.1(6)	−5.0(3)	11.5(7)	105
	0.08(3)	−8(3)	–	4.0(2)	−10.71(5)	3.3(1)	52
	< 0.009			8.8(7)	−11.8(1)	26.9(5)	> 978
				0.11(2)	−17(9)	141(31)	> 12
				1.8(4)	−17.6(2)	5.0(7)	> 200
	0.05(1)	−25(4)	–	7.2(3)	−23.59(8)	7.4(2)	148
				0.18(2)	−113(2)	34(5)	> 20

Source	**HI Absorption** (GMRT)			**HI Emission** (LDS)			
	$\tau_{\rm HI}$	$V_{\rm lsr}$ (km s^{-1})	FWHM (km s^{-1})	T_B (K)	$V_{\rm lsr}$ (km s^{-1})	FWHM (km s^{-1})	T_S (K)
J2009 + 724	0.20(2)	−5.2(1)	–	22.8(1)	−5.11(1)	9.54(5)	126
	< 0.009			7.0(1)	−10.1(2)	29.2(3)	> 778
				3.4(1)	−22.23(8)	8.3(3)	> 378
				3.9(2)	−52.9(2)	21.5(5)	> 433
				1.7(2)	−55.1(1)	8.7(6)	> 189
				0.83(2)	−123.6(4)	35(1)	> 92
J2011 − 067	< 0.006			0.57(2)	+53.6(7)	27(2)	> 95
				0.40(4)	+30.6(6)	11(1)	> 44
	0.020(3)	+11.1(6)	–	0.8(1)	+9.9(2)	4.9(8)	40
				4.4(2)	+4.4(1)	23.9(4)	> 733
	0.058(1)	+0.1(2)	7.2(4)	5.9(3)	+1.25(4)	3.7(1)	105
				9.7(1)	−2.93(7)	6.5(1)	> 1617
J2047 − 026	< 0.006			1.1(4)	−2(1)	5(1)	> 183
	0.035(3)	+6(1)	4(2)	4.7(5)	+2.0(2)	4.4(2)	134
				4.2(3)	+3.9(0.2)	19(1)	> 700
	0.012(4)	+13(3)	5(7)	0.8(1)	+9.4(3)	4.9(9)	67
				1.1(0.3)	+18(5)	33(5)	> 183
				0.30(4)	+35.5(3)	4.7(8)	> 50
				0.10(1)	+48(8)	50(5)	> 17
J2130 + 050	0.10(1)	+01.40(7)	3.8(1)	16.3(2)	+00.60(3)	6.7(1)	163
	< 0.006			4.1(2)	+06.1(4)	18.1(8)	> 683
				1.3(2)	+14(2)	50(3)	> 216
J2136 + 006	0.14(2)	0(2)	–	8.6(1)	+00.8(4)	6.0(1)	61
	0.10(5)	+05.5(1)	4.7(4)	8.5(1)	+06.20(3)	4.0(1)	85
	< 0.006			6.9(1)	+04.80(6)	19.6(2)	> 1150
				0.40(2)	−36.0(8)	23(2)	> 67
J2137 − 207	0.025(2)	−1.2(3)	3.8(5)	3.7(2)	+1.03(4)	7.1(1)	150
	< 0.006			3.6(1)	−0.6(1)	15.7(6)	> 600
				2.4(2)	−3.7(2)	29.3(6)	> 400
J2148 + 069	< 0.006			7.8(1)	−7.62(4)	5.92(9)	> 1300
	0.079(3)	−2.1(2)	8.0(4)	6.7(3)	+0.63(9)	11.2(3)	88
				4.3(3)	+2.3(2)	23.6(5)	> 717
	0.040(4)	+7.7(2)	–				
J2212 + 018	< 0.003			0.08(1)	+35(8)	109(12)	> 27
	0.016(1)	+7.0(9)	14(2)	4.5(1)	+0.32(8)	11.2(3)	284
				3.4(1)	−1.7(1)	24.2(4)	> 1133
	0.037(4)	−3.6(2)	–	6.05(8)	−7.23(2)	4.64(6)	167
J2214 − 385	< 0.006			No data			

Source	**HI Absorption** (GMRT)			**HI Emission** (LDS)			
	$\tau_{\rm HI}$	$V_{\rm lsr}$ (km s^{-1})	FWHM (km s^{-1})	T_B (K)	$V_{\rm lsr}$ (km s^{-1})	FWHM (km s^{-1})	T_S (K)
J2219 − 279	< 0.009			0.7(4)	−13.2(4)	11(2)	> 78
				1.4(5)	−4(2)	18(4)	> 156
				0.6(4)	−3.9(7)	32(4)	> 67
J2225 − 049	< 0.009			0.15(2)	−10(3)	60(6)	> 17
				9.2(2)	−5.24(9)	5.09(1)	> 1022
				2.8(4)	−2.50(5)	2.8(2)	> 200
	0.124(4)	−2.4(1)	5.4(3)	10.15(7)	+0.15(7)	15.2(1)	87
	0.029(4)	+8(2)	–	1.25(8)	+8.77(6)	3.4(2)	44
				0.68(4)	+16.8(1)	4.8(4)	> 76
J2232 + 117	< 0.009			9.87(8)	+0.6(1)	14.1(2)	> 1097
				0.77(5)	−3.4(0.6)	50(2)	> 86
	0.079(3)	−4.6(2)	8.3(5)	7.4(2)	−5.81(2)	5.3(1)	94
	0.040(4)	−15.3(3)	–	3.83(7)	−13.88(3)	3.92(8)	96
J2236 + 284	< 0.012			4(1)	+5(2)	14(2)	> 333
	0.018(4)	−1(1)	12(4)	8(2)	−0.16(4)	8.7(4)	448
				0.6(1)	0(3)	51(4)	> 50
	0.031(5)	−14.2(6)	5(1)	3.6(2)	−11.0(2)	10.1(3)	118
				1.5(1)	−24.3(2)	12.3(7)	> 125
				0.64(5)	−61.0(3)	13.5(9)	> 53
				0.61(4)	−68(2)	40(2)	> 51
J2246 − 121	< 0.009			4.36(6)	+3.84(3)	4.67(6)	> 484
				7.33(9)	−1.31(3)	21.6(1)	> 814
	0.016(3)	−2.9(9)	8(2)	4.93(8)	−3.46(3)	7.05(9)	308
J2250 + 143	0.037(3)	−4.2(3)	5.0(6)	5.7(1)	−2.02(2)	4.06(7)	157
	< 0.006			8.6(1)	−2.52(3)	13.9(1)	> 1433
				0.91(3)	−13.2(9)	53(2)	> 152
				2.01(5)	−15.34(6)	5.2(2)	> 335
				0.38(4)	−40.7(5)	13(2)	> 63
J2251 + 188	0.041(4)	−0.3(3)	7.3(9)	14.74(8)	−0.27(2)	10.51(6)	367
	< 0.006			1.88(8)	−7.5(4)	30.0(9)	> 313
	0.015(3)	−9(3)	22(3)	1.47(8)	−8.6(1)	5.4(3)	99
J2302 − 373	< 0.006			No data			
J2340 + 135	< 0.006			2.12(9)	+4.84(7)	4.4(2)	> 353
				2.3(2)	−2.20(6)	3.0(2)	> 383
	0.216(5)	−4.60(7)	3.5(1)	9.1(2)	−4.58(7)	15.5(1)	47
	0.098(5)	−11(3)	–	5.8(1)	−6.27(5)	5.6(1)	62
				1.41(2)	−36.2(2)	27.9(5)	> 235
J2341 − 351	< 0.012			No data			

References

Albert, C. E. 1983, *Astrophys. J.*, **272**, 509.
Brand, J., Blitz, L. 1993, *Astron. Astrophys.*, **275**, 67.
Burton, W. B. 1988, in *Galactic and Extragalactic Radio Astronomy*, (eds) G. L. Verschuur & K. I. Kellermann (New York: Springer-Verlag), p. 295.
Clark, B. G., Radhakrishnan, V., Wilson, R. W. 1962, *Astrophys. J.*, **135**, 151.
Clark, B. G. 1965, *Astrophys. J.*, **142**, 1398.
Dickey, J. M., Salpeter, E. E., Terzian, Y. 1978, *Astrophys. J. Suppl.*, **36**, 77.
Dickey, J. M., Benson, J. M. 1982, *Astron. J.*, **87**, 278.
Dickey, J. M., Kulkarni, S. R., Heiles, C. E., van Gorkom, J. H. 1983, *Astrophys. J. Suppl.*, **53**, 591.
Dickey, J. M., Lockman, F. J. 1990, *Ann. Rev. Astron. Astrophys.*, **28**, 215.
Field, G. B., Goldsmith, D. W., Habing, H. J. 1969, *Astrophys. J. Lett.*, **155**, L149.
Hartmann, D., Burton, W. B. 1995, *An Atlas of Galactic Neutral Hydrogen*, Cambridge Univ. Press.
Heiles, C., Troland, T. H. 2003a, *Astrophys. J. Suppl.*, **145**, 329.
Heiles, C., Troland, T. H. 2003b, *Astrophys. J.*, **586**, 1067.
Kalberla, P. M. W., Westphalen, G., Mebold, U., Hartmann, D., Burton, W.B. 1998, *Astron. Astrophys. Lett.*, **332**, L61.
Lockman, F. J., Gehman, C. S. 1991, *Astrophys. J.*, **382**, 182.
Mebold, U., Winnberg, A., Kalberla, P. M. W., Goss, W. M. 1981, *Astron. Astrophys. Suppl.*, **46**, 389.
Mebold, U., Winnberg, A., Kalberla, P. M. W., Goss, W. M. 1982, *Astron. Astrophys.*, **115**, 223.
Mohan, R., Dwarakanath, K. S., Srinivasan, G. 2004 (Paper II), *J. Astrophys. Astron.*, (this volume).
Radhakrishnan, V., Murray, J. D., Lockhart, P., Whittle, R. P.J. 1972a, *Astrophys. J. Suppl.*, **24**, 15.
Radhakrishnan, V., Goss, W. M., Murray, J. D., Brooks, J. W. 1972b, *Astrophys. J. Suppl.*, **24**, 49.
Radhakrishnan, V., Goss, W. M. 1972, *Astrophys. J. Suppl.*, **24**, 161.
Spitzer, L. Jr. 1978, *Physical Processes in the interstellar Medium*, New York: Wiley Interscience.
Swarup, G., Ananthakrishnan, S., Kapahi, V. K., Rao, A. P., Subrahmanya, C. R., Kulkarni, V. K. 1991, *Current Science*, **60**, 95.
Wolfire, M. G., Hollenbach, D., McKee, C. F., Tielens, A. G. G. M., Bakes, E. L. O. 1995, *Astrophys. J.*, **443**, 152.